A Low-Valent Molybdenum Nitride: Reduction Promotes Carbonylation Chemistry

Joshua A. Buss, Christine Cheng, and Theodor Agapie*

Division of Chemistry and Chemical Engineering, California Institute of Technology, 1200 East California Boulevard, MC 127-72, Pasadena, California 91125, United States

Supporting Information

Contents

Experimental Details

General Considerations

Unless otherwise specified, all operations were carried out in an MBraun drybox under a nitrogen atmosphere or using standard Schlenk and vacuum line techniques. Solvents for air- and moisture-sensitive reactions were dried over sodium benzophenone ketyl, calcium hydride, or by the method of Grubbs.[1] Deuterated solvents were purchased from Cambridge Isotope Laboratories and vacuum transferred from sodium benzophenone ketyl (C_6D_6, C_7D_8), CaH_2 (CD_2Cl_2), or used without further purification (D_2O). Solvents, once dried and degassed, were vacuum transferred directly prior to use or stored under inert atmosphere over activated 4 Å molecular sieves. **1**[2] was prepared according to a literature procedure. Unless indicated otherwise, all chemicals were used as received. $TBAN_3$ (dried under vac. at 40 °C for 8 h), $Na^{15}N_3$ [50% terminal ^{15}N] (dried under vac. at 60 °C for 8h), naphthalene (vacuum sublimed at 40 °C), ^{13}CO, Me_3SiOTf, and ^{t}BuNC were purchased from Sigma Aldrich. Na^0 (washed with hexanes under N_2 to remove oil) and K^0 (washed with hexanes under N_2 to remove oil) were purchased from Alfa Aesar and Acros, respectively. ^1H, $^{13}C\{^1H\}$, and $^{31}P\{^1H\}$ NMR spectra were recorded on a Varian 400 MHz or Varian INOVA-500 spectrometers with shifts reported in parts per million (ppm). ^1H and $^{13}C\{^1H\}$ NMR spectra are referenced to residual solvent peaks.[3] $^{31}P\{^1H\}$ chemical shifts are referenced to an external 85% H_3PO_4 (0 ppm) standard. $^{15}N\{^1H\}$ chemical shifts are referenced to an external CD_3NO_2 (380.23 ppm) standard. Multiplicities are abbreviated as follows: s = singlet, d = doublet, dd = doublet of doublets, t = triplet, vt = virtual triplet, q = quartet, app dq = apparent doublet of quartets, m = multiplet, br = broad, v br = very broad. Elemental analysis was performed at the Caltech XRCF using a PerkinElmer 2400 Series II CHN Elemental Analyzer.

Synthesis of 2

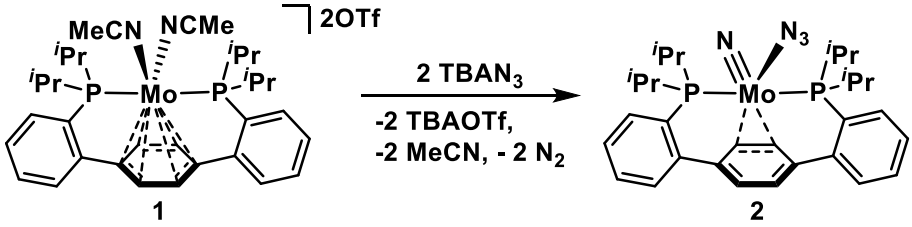

A 100 mL RB flask was charged with **1** (2 g, 2.13 mmol) and a stir bar. MeCN (40 mL) was added and stirring was initiated, affording a dark purple homogeneous solution. A solution of $TBAN_3$ (1.27 g, 4.47 mmol) in MeCN (10 mL) was added dropwise. The purple solution gradually turned deep maroon and gas evolution was evident. With prolonged stirring, formation of a brick red precipitate was observed. After 2.5 h, the solvent volume was concentrated to *ca.* 10 mL under reduced pressure. While still cold, the resulting suspension was filtered on a medium porosity sintered glass frit. The solids were washed with -35 °C MeCN (7 mL x 3), dried *in vacuo*, and collected, providing analytically pure **2** as a free-flowing red powder (1.1 g, 1.80 mmol, 84%). X-ray quality single crystals were grown via vapor diffusion of pentane into a concentrated toluene solution of **2**. ^1H NMR (400 MHz, C_6D_6, 23 °C) δ: 7.31 (app dq, J = 7.1 & 1.5 Hz, 2H, aryl-*H*), 7.22-7.25 (m, 2H, aryl-*H*), 7.13-7.16 (m, 2H, aryl-*H*), 7.07-7.11 (m, 2H, aryl-*H*), 5.93 (br s, 2H, central arene-*H*), 4.43 (t, J = 2.3 Hz, 2H, central arene-*H*), 3.01-3.12 (m, 2H, C*H*$(CH_3)_2$), 2.47-2.61 (m, 2H, C*H*$(CH_3)_2$), 1.94-2.00 (m, 6H, CH(C*H*$_3)_2$), 1.38-1.44 (m, 6H, CH(C*H*$_3)_2$), 0.72-0.76 (m, 6H, CH(C*H*$_3)_2$), 0.28-0.34 (m, 6H, CH(C*H*$_3)_2$). $^{13}C\{^1H\}$ NMR (101 MHz, C_6D_6, 23 °C) δ: 150.88 (vt, J = 6.99, aryl-*C*), 140.99 (vt, J = 4.94 Hz, central arene-*C*), 132.07 (s, aryl-*C*), 130.79 (s, aryl-*C*), 127.64 (vt, J = 2.34 Hz, aryl-*C*), 127.35 (vt, J = 2.48 Hz, aryl-*C*), 122.58 (vt, J = 15.45 Hz, aryl-*C*), 121.95 (s, central arene-*C*), 62.13 (vt, J = 2.54 Hz, central arene-*C*), 23.19 (vt, J = 8.15 Hz, *C*H$(CH_3)_2$), 22.47 (vt, J = 8.73 Hz, *C*H$(CH_3)_2$), 18.60 (br s, CH(*C*H$_3)_2$), 17.31 (vt, J = 2.71 Hz, CH(*C*H$_3)_2$), 17.18 (vt, J = 4.59 Hz, CH(*C*H$_3)_2$), 15.59 (br s, CH(*C*H$_3)_2$). $^{31}P\{^1H\}$ NMR (162 MHz, C_6D_6, 23 °C) δ: 35.01 (s). Despite triplicate

measurements, satisfactory EA of **2** was not obtained. Anal. Calcd. for **2** $C_{30}H_{40}MoN_4P_2$ (%): C, 58.6; H, 6.6; N, 9.1. Found (ave.): C, 57.4; H, 6.5; N, 10.2.

^{15}N enriched (50%) **2** can be obtained following a similar procedure utilizing $Na^{15}N_3$ in lieu of $TBAN_3$. However, the reaction takes longer (14 h), as the $Na^{15}N_3$ is not completely soluble in the MeCN solvent. Moreover, prepared this way, **2** contains a free diphsophine impurity that must be washed away with cold pentane, reducing the isolated yield.

$^{15}N\{^1H\}$ NMR (51 MHz, C_6D_6, 25 °C) δ: 833.09 (s, Mo≡*N*), 137.23 ppm (s, Mo-N_3(*αN*)), 62.23 ppm (s, Mo-N_3(*γN*)).

*Synthesis of **3***

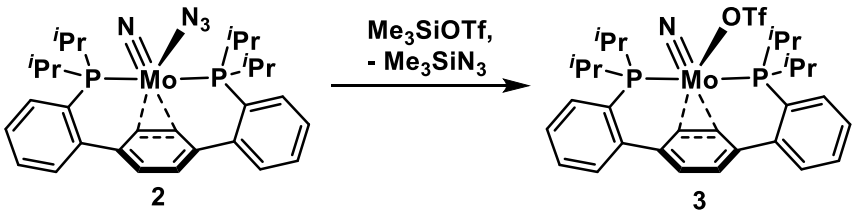

2 **3**

To a 20 mL scintillation vial charged with **2** (600 mg, 0.976 mmol) and a stir bar, C_6H_6 (12 mL) was added. Stirring was initiated and Me_3SiOTf (260 mg, 1.17 mmol) was added, resulting in a subtle lightening of the reaction mixture. Stirring continued for 1 h, at which time a *ca.* 0.5 mL aliquot was removed and analyzed by $^{31}P\{^1H\}$ NMR spectroscopy. In some cases, residual **2** was observed spectroscopically, and additional Me_3SiOTf (1.2 equiv. based off of relative integration of **2** to **3** in the $^{31}P\{^1H\}$ NMR spectrum of the reaction aliquot) was added. Once complete conversion was observed, the vial was placed in the freezer (-35 °C) and the contents frozen solid. Lyophilization of the C_6H_6 afforded a flocculent pink powder. This powder was triturated with (2 mL x 2) and then suspended in (*ca.* 4 mL) hexanes. The hexanes suspension as cooled to -35 °C and the solids were collected on a coarse frit. Removal of the volatiles under reduced pressure provided **3** as a reddish pink powder (493 mg, 0.685 mmol, 70%). ^1H NMR (400 MHz, C_6D_6, 23 °C) δ: 7.31 (br d, *J* = 6.69 Hz, 2H, aryl-*H*), 7.26 (br d, *J* = 6.92 Hz, 2H, aryl-*H*), 7.14-7.18 (m, 2H, aryl-*H*), 7.08-7.12 (m, 2H, aryl-*H*), 6.07 (s, 2H, central arene-*H*), 4.19 (br t, *J* = 2.04 Hz, 2H, central arene-*H*), 3.43-3.49 (m, 2H, C*H*$(CH_3)_2$), 2.56-2.66 (m, 2H, C*H*$(CH_3)_2$), 2.02-2.08 (m, 6H, CH(C*H*$_3)_2$), 1.29-1.35 (m, 6H, CH(C*H*$_3)_2$), 0.84-0.88 (m, 6H, CH(C*H*$_3)_2$), 0.26-0.32 (m, 6H, CH(C*H*$_3)_2$). $^{13}C\{^1H\}$ NMR (101 MHz, C_6D_6, 23 °C) δ: 149.80 (vt, *J* = 6.46 Hz, aryl-*C*), 140.99 (vt, *J* = 4.77 Hz, aryl-*C*), 132.06 (s, aryl-*C*), 130.71 (s, aryl-*C*), 127.85 (aryl-*C*; coincides with C_6D_6 residual but observed via 2D NMR spectroscopy), 127.11 (vt, *J* = 2.54 Hz, aryl-*C*), 123.10 (vt, *J* = 16.58 Hz, aryl-*C*), 122.53 (s, central arene-*C*), 120.36 (q, *J* = 318.47 Hz, *C*F_3), 63.97 (s, central arene-*C*), 24.34 (t, *J* = 8.96 Hz, *C*H$(CH_3)_2$), 22.19 (m, *C*H$(CH_3)_2$), 18.62 (d, *J* = 40.92 Hz, CH(*C*H$_3)_2$), 17.91 (m, CH(*C*H$_3)_2$), 17.65 (m, CH(*C*H$_3)_2$), 15.78 (d, *J* = 13.14 Hz, CH(*C*H$_3)_2$). $^{31}P\{^1H\}$ NMR (162 MHz, C_6D_6, 23 °C) δ: 34.42 (s). ^{19}F NMR (376 MHz, C_6D_6, 23 °C): -76.91 (s). Despite triplicate measurements, satisfactory EA of **3** was not obtained. Anal. Calcd. for **3** $C_{31}H_{40}F_3MoNO_3P_2S$ (%): C, 51.6; H, 5.6; N, 1.9. Found (ave.): C, 50.5; H, 5.5; N, 2.8.

^{15}N enriched (50%) **3** can be obtained following a similar procedure starting from enriched **2**.

$^{15}N\{^1H\}$ NMR (51 MHz, C_6D_6, 25 °C) δ: 842.22 (s, Mo≡*N*).

*In situ Preparation of **4***

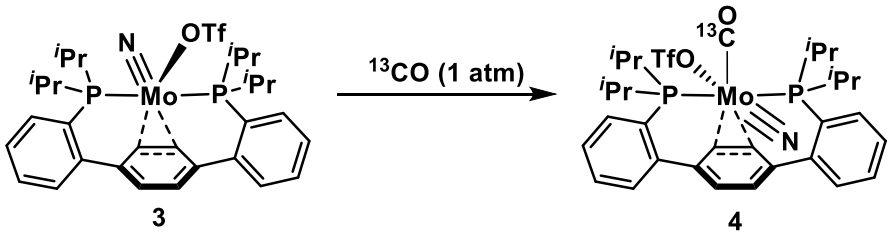

3 **4**

A J. Young style NMR tube was charged with a deep red C_6D_6 (0.5 mL) solution of **3** (20 mg, 0.028 mmol). The tube was degassed via three freeze-pump-thaw cycles and the atmosphere was replaced with CO. Following mixing, the solution color changed from deep red to orange. Upon standing for 8 h, X-ray quality red/orange microcrystals of **4** formed. Further reactivity was probed using samples of **4** prepared in this fashion. The solubility of **4** in PhMe or THF was not significantly improved; **4** was more soluble in CD_2Cl_2, but slowly decomposed to an intractable mixture in this solvent.

An IR spectrum of **4** was obtained following precipitation from THF solution, decantation of the mother liquor, and briefly drying the resulting solids *in vacuo*. Prepared this way, a strong CO stretch was observed via ATR IR Spectrsocopy—ν_{CO}: 1980 cm^{-1}.

4-^{13}C was prepared analogously using ^{13}CO in lieu of CO.

The room temperature spectra of **4-^{13}C** are broad, suggesting an exchange process that is intermediate on the NMR timescale. ^{1}H NMR (400 MHz, CD_2Cl_2, 23 °C) δ: 7.94 (br s, 2H, aryl-*H*), 7.69 (br s, 6H, aryl-*H*), 7.16 (br s, 2H, central arene-*H*), 6.93 (v br, 2H, central arene-*H*), 2.94 (v br, 2H, C*H*$(CH_3)_2$), 2.83 (v br, 2H, C*H*$(CH_3)_2$), 0.88-1.34 (br m, 24H, CH(C*H*$_3)_2$). ^{13}C{^{1}H} NMR (101 MHz, C_6D_6, 23 °C) δ: 238.43 (v br, Mo-*C*O). ^{31}P{^{1}H} NMR (162 MHz, C_6D_6, 23 °C) δ: 38.74 (br s). ^{19}F NMR (376 MHz, C_6D_6, 23 °C): -76.69 (s).

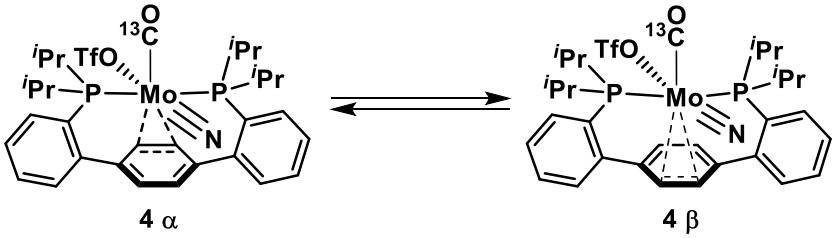

4 α **4** β

Spectra of the same sample collected at -80 °C show two distinct species, approaching the slow exchange limit. This process is attributed to the Mo center slipping across the face of the arene, interconverting the coordination isomers (**α** and **β**) shown above. ^{1}H NMR (500 MHz, CD_2Cl_2, -65 °C) δ: 7.94 (br s, 2H, aryl-*H*), 7.89 (br s, 2H, aryl-*H*), 7.73 (br t, *J* = 6.6 Hz, 4H, aryl-*H*), 7.65-7.66 (br m, 8H, aryl-*H*), 7.43 (s, 2H, central arene-*H*), 7.31 (s, 2H, central arene-*H*), 6.91 (br s, 2H, central arene-*H*), 6.37 (br t, *J* = 5.4 Hz, 2H, central arene-*H*), 3.24 (br m, 2H, C*H*$(CH_3)_2$), 3.11 (br m, 2H, C*H*$(CH_3)_2$), 2.54 (br m, 4H, C*H*$(CH_3)_2$), 1.50-1.56 (m, 12H, CH(C*H*$_3)_2$), 1.43-1.48 (m, 6H, CH(C*H*$_3)_2$), 1.37-1.41 (m, 6H, CH(C*H*$_3)_2$), 1.40 (br m, 6H, CH(C*H*$_3)_2$), 0.89 (br m, 6H, CH(C*H*$_3)_2$), 0.77-0.78 (br m, 6H, CH(C*H*$_3)_2$), 0.12-0.14 (br m, 6H, CH(C*H*$_3)_2$). ^{13}C{^{1}H} NMR (126 MHz, C_6D_6, -65 °C) δ: 244.84 (br t, *J* = 10.1 Hz, Mo-*C*O), 234.62 (br s, Mo-*C*O). ^{31}P{^{1}H} NMR (202 MHz, C_6D_6, -65 °C) δ: 39.02 (v br), 38.53 (v br). Due to the lability of the CO ligand, EA of **4** was forgone.

*Synthesis of **5***

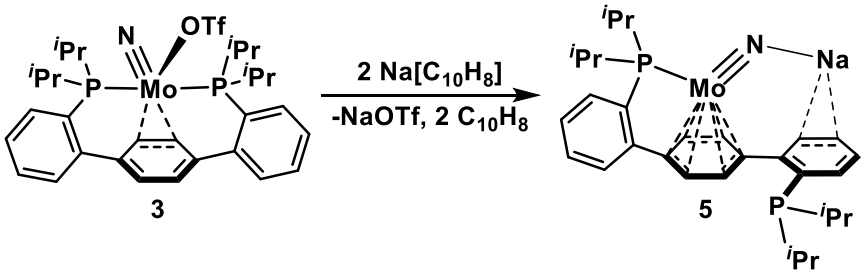

A $Na[C_{10}H_8]$ solution was prepared by stirring a $C_{10}H_8$ (196 mg, 1.53 mmol) solution in THF (6 mL) in a 20 mL scintillation vial charged with a Na^0 mirror for 2 h.

During this time, a second scintillation vial was charged with **3** (500 mg, 0.695 mmol), THF (6 mL), and a stir bar. The vial was placed in an LN_2 chilled cold well and the contents frozen solid. Immediately upon thawing, with stirring, the aforementioned $Na[C_{10}H_8]$ solution was added dropwise. Following addition, the Na^0 mirror was rinsed with THF (1 mL x 2) and these washes were likewise added to the reaction vial. Stirring continued for 20 minutes, affording a dark red, homogeneous solution. Volatiles were removed under reduced pressure, providing a tacky red/brown residue. This residue was triturated with hexanes (4 mL) and the resulting red/brown solids suspended in hexanes (5 mL). The mixture was filtered through a medium porosity fritted funnel and the filtrant was washed thoroughly with hexanes (3 x 7 mL) to remove residual $C_{10}H_8$. The solids were collected and dried *in vacuo*, providing **5-Na** as a free-flowing deep red solid (320 mg, 0.535 mmol, 77%). ^{1}H NMR (400 MHz, C_6D_6, 23 °C) δ: 9.08 (t, *J* = 7.41 Hz, 1H, aryl-*H*), 8.44 (dd, *J* = 7.04 & 3.71 Hz, 1H, aryl-*H*), 7.41 (d, *J* = 7.62 Hz, 1H, aryl-*H*), 7.35 (dd, *J* = 7.79 & 2.85 Hz, 1H, aryl-*H*), 7.16-7.21 (2H, aryl-*H*; partially coincides with the C_6D_5H residual but observed via 2D NMR), 6.98 (t, *J* = 7.60 Hz, 1H, aryl-*H*), 6.91 (t, *J* = 7.43 Hz, 1H, aryl-*H*), 5.85 (d, *J* = 5.73 Hz, 1H, central arene-*H*), 5.24 (d, *J* = 5.70 Hz, 1H, central arene-*H*), 5.04 (t, *J* = 4.89 Hz, 1H, central arene-*H*), 5.00 (t, *J* = 5.04 Hz, 1H, central arene-*H*), 2.46-2.55 (m, 1H, C*H*$(CH_3)_2$), 2.18-2.28 (m, 1H, C*H*$(CH_3)_2$), 2.00-2.09 (m, 1H, C*H*$(CH_3)_2$), 1.86-1.94 (m, 1H, C*H*$(CH_3)_2$), 1.59-1.65 (m, 3H, CH(C*H*$_3)_2$), 1.48-1.53 (m, 3H, CH(C*H*$_3)_2$), 1.35-1.40 (m, 3H, CH(C*H*$_3)_2$), 1.24-1.29 (m, 3H, CH(C*H*$_3)_2$), 1.02-1.07 (m, 3H, CH(C*H*$_3)_2$), 0.92-1.07 (m, 3H, CH(C*H*$_3)_2$), 0.88-0.93 (m, 3H, CH(C*H*$_3)_2$), 0.54-0.60 (m, 3H, CH(C*H*$_3)_2$). ^{13}C{^{1}H} NMR (101 MHz, C_6D_6, 23 °C) δ: 152.05 (d, *J* = 24.05 Hz, aryl-*C*), 150.80 (d, *J* = 24.54 Hz, aryl-*C*), 138.14 (d, *J* = 25.96 Hz, aryl-*C*), 137.52 (d, *J* = 38.91 Hz, aryl-*C*), 132.91 (d, *J* = 2.29 Hz, aryl-*C*), 131.56 (s, aryl-*C*), 130.67 (d, *J* = 4.05 Hz, aryl-C), 126.52 (dd, *J* = 3.62 & 1.56 Hz, aryl-*C*), 124.74 (s, aryl-*C*), 93.26 (d, *J* = 5.16 Hz, central arene-*C*), 78.95 (d, *J* = 47.48 Hz, central arene-*C*), 75.30 (d, *J* = 7.60 Hz, central arene-*C*), 72.64 (s, central arene-*C*), 67.69 (d, *J* = 17.38 Hz, central arene-*C*), 29.28 (d, *J* = 13.01 Hz, *C*H$(CH_3)_2$), 26.91 (d, *J* = 13.59 Hz, *C*H$(CH_3)_2$), 26.02 (d, *J* = 19.38 Hz, *C*H$(CH_3)_2$), 22.69 (d, *J* = 9.99 Hz, CH(*C*H$_3)_2$), 22.15 (d, *J* = 15.31 Hz, *C*H$(CH_3)_2$), 21.51 (d, *J* = 18.87 Hz, CH(*C*H$_3)_2$), 20.37 (d, *J* = 12.97 Hz, (CH(*C*H$_3)_2$), 20.15 (d, *J* = 22.10 Hz, CH(*C*H$_3)_2$), 19.88 (d, *J* = 3.08 Hz, CH(*C*H$_3)_2$), 19.62 (s, CH(*C*H$_3)_2$), 19.06 (d, *J* = 11.89 Hz, CH(*C*H$_3)_2$), 18.83 (d, *J* = 6.58 Hz, CH(*C*H$_3)_2$). ^{31}P{^{1}H} NMR (162 MHz, C_6D_6, 23 °C) δ: 53.73 (s, Mo-*P*), -2.04 (s, *P*). Despite triplicate measurements, satisfactory EA of complex **5** was not obtained, likely due to the air and moisture sensitivity of the highly reduced complex.

5-K can be prepared analogously using $K[C_{10}H_8]$ in lieu of $Na[C_{10}H_8]$. The spectroscopic features are identical to those of **5-Na**. Single crystals of **5-K** were grown via vapor diffusion of hexanes into a concentrated C_6H_6 solution.

^{15}N enriched (50%) **5** can be obtained following a similar procedure starting from enriched **3**.

^{15}N{^{1}H} NMR (51 MHz, C_6D_6, 25 °C) δ: 735.63 (s, Mo≡*N*).

Reactions from **4**

^{13}CO Dissociation

A J. Young NMR tube was charged with a deep red C_7D_8 (0.4 mL) solution of **3** (20 mg, 0.028 mmol). The solution was degassed via three freeze-pump-thaw cycles and placed under *ca.* 0.4 atm of ^{13}CO. The reaction mixture was mixed via inversion for 2 h, at which time the solution color had become bright orange and a significant amount of orange precipitate had formed; $^{31}P\{^1H\}$ NMR spectroscopy showed partial conversion to **4** (**4** comprised 63% of the soluble diamagnetic material; however, significant precipitation of **4** was likewise observed). Inversion mixing continued for an additional 14 h, resulting in lightening of the solution. At this time, minor decomposition to an unknown species was observed (Figure S1, *) by ^{1}H NMR spectroscopy.

The contents of the J. Young tube were degassed via three freeze-pump-thaw cycles and mixed for 2 h. ^{1}H NMR spectroscopy demonstrated significant growth of CO-free **3**, confirming ^{13}CO loss from **4-^{13}C**.

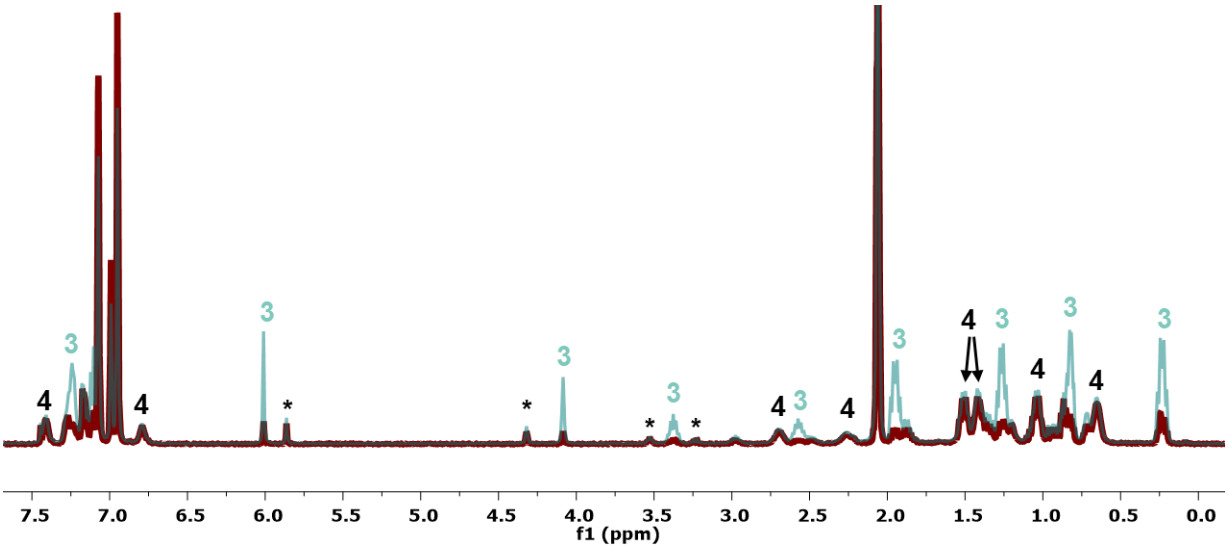

Figure S1—^{1}H NMR spectra of a mixture of **3**, **4-^{13}C**, and an unidentified decomposition product (*) under ^{13}CO (maroon trace) and after evacuation of the headspace (blue trace). The relative intensity of **3** increases *ca.* fourfold, relative to the solvent residual, after degassing. The relative concentration of **4-^{13}C** remains roughly constant as the solution is saturated throughout.

Two-Electron Reduction

A J. Young NMR tube was charged with a deep red C_6H_6 (0.4 mL) solution of **3** (20 mg, 0.028 mmol). The solution was degassed via three freeze-pump-thaw cycles and placed under 1 atm of CO. The reaction mixture was mixed via inversion for 2 h, at which time the solution color had become bright orange and a significant amount of orange precipitate had formed; $^{31}P\{^1H\}$ NMR spectroscopy showed near complete consumption of the starting material and conversion to **4** (>93%).

During *in situ* formation of **4**, a Na[$C_{10}H_8$] solution was prepared by stirring a THF (0.4 mL) solution of $C_{10}H_8$ (7.5 mg, 0.059 mmol) over a Na^0 mirror. With a strong Ar counterflow, the deep green Na[$C_{10}H_8$] solution was added to the J. Young tube. The tube was sealed, mixed vigorously, and the contents analyzed by $^{31}P\{^1H\}$ NMR spectroscopy.

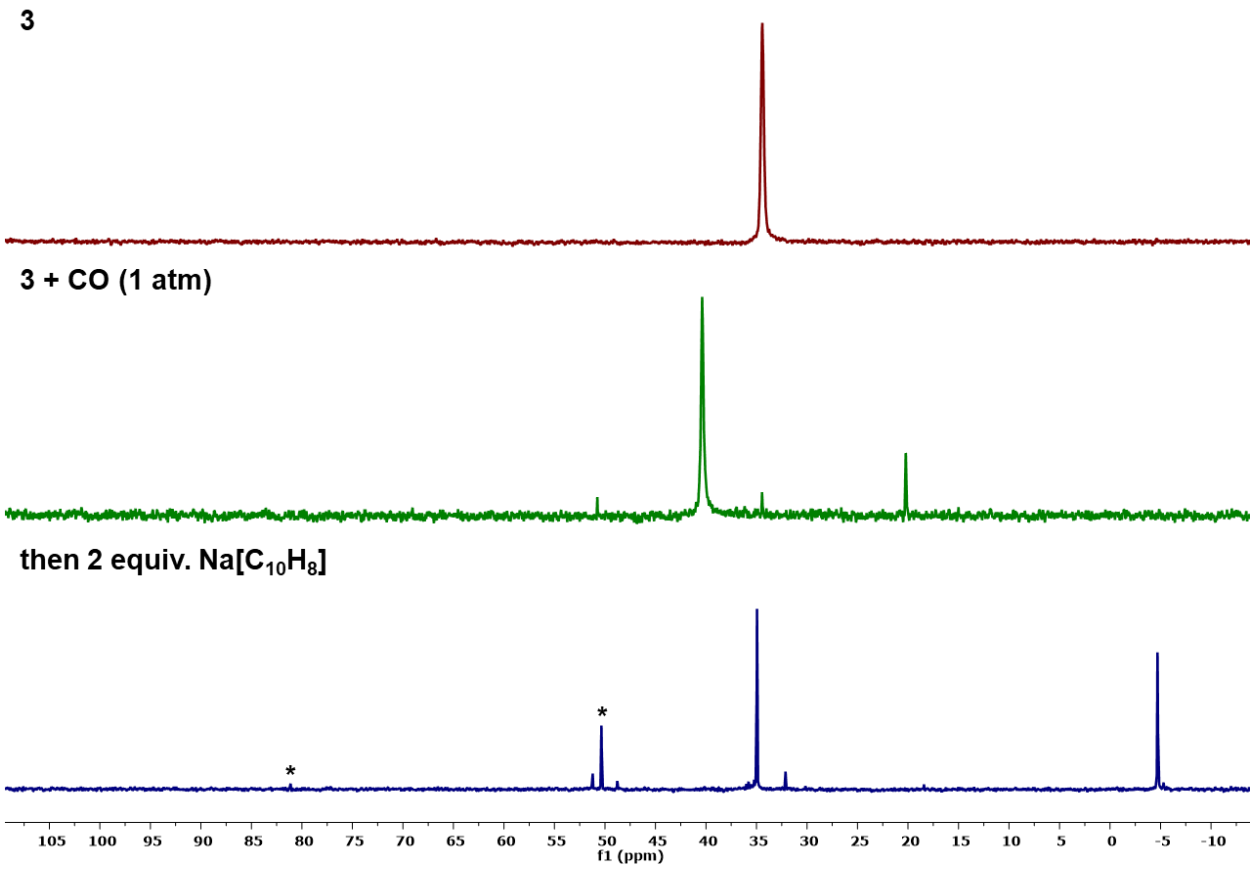

Figure S2—$^{31}P\{^{1}H\}$ NMR spectra (162 MHz, THF, 23 °C) monitoring sequential CO addition and reduction of nitride triflate complex **3**. Upon two-electron reduction, significant decomposition to free diphosphine is observed, in addition to significant reversion to CO-free starting material, **3**. Minor conversion to N^- group transfer products, **C** and **D** (denoted with asterisks), was observed.

Nitride Carbonylation Reactions

*Addition of ^{13}CO to **5***

A 50 mL Teflon stoppered Schlenk tube was charged with **5-Na** (40 mg, 0.067 mmol), THF (5 mL), and a stir bar. The flask was sealed and attached to a 33.4 mL calibrated volume. The reaction mixture was thoroughly degassed via three freeze-pump-thaw cycles. Following thawing the final time, the Schlenk tube was submerged in a -78 °C dry ice/acetone slush bath. Using a Hg manometer, 14.7 cm Hg of ^{13}CO was admitted to the calibrated volume (0.268 mmol). The ^{13}CO was then introduced to the reaction flask, which was allowed to warm to room temperature, with stirring, over the course of 12 h. At this time, volatiles were removed under reduced pressure, leaving red/orange solids. This residue was extracted with C_6H_6 (2 mL) and then set aside. The C_6H_6 fraction was pumped to dryness and analyzed by multinuclear NMR, evincing formation of Mo(0) carbonyl complexes in addition to free diphosphine. The insoluble material was taken up in D_2O (0.5 mL) and analyzed by $^{13}C\{^1H\}$ NMR spectroscopy, demonstrating formation of $NaN^{13}CO$.

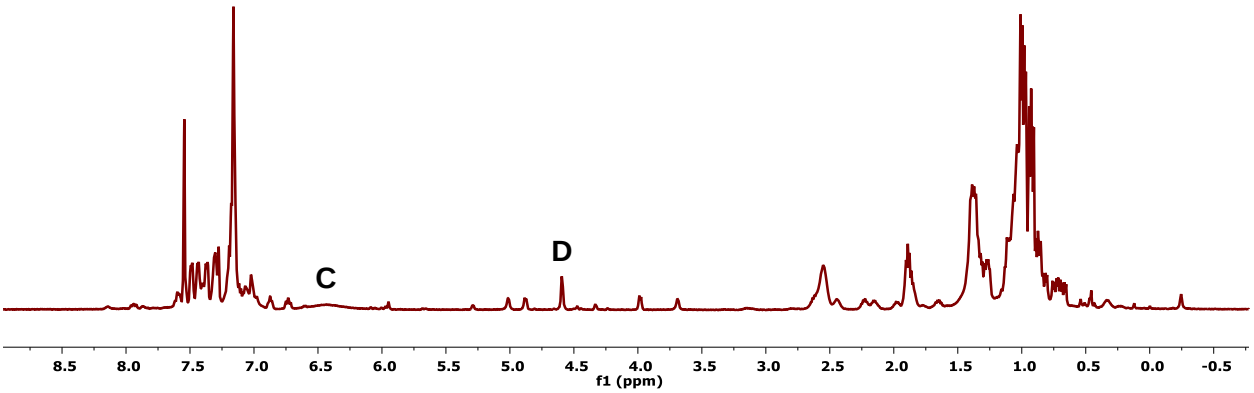

Figure S3—^1H NMR spectrum (500 MHz, C_6D_6, 25 °C) of the C_6H_6 soluble reaction products following ^{13}CO addition to **5-Na**. The central arene resonances of carbonyl complexes P2Mo(^{13}CO)$_3$ [**C**] and P2Mo(^{13}CO) [**D**] are labeled.

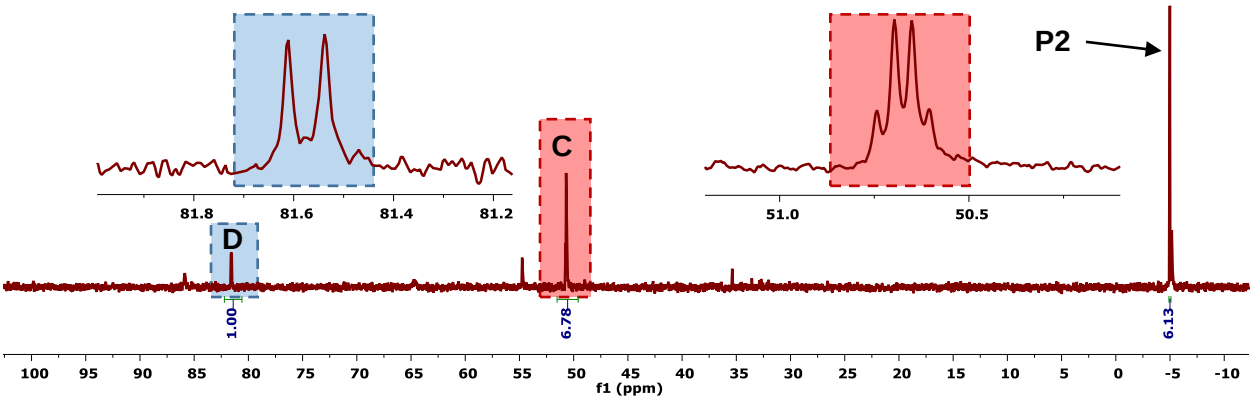

Figure S4—$^{31}P\{^1H\}$ NMR spectrum (202 MHz, C_6D_6, 25 °C) of the C_6H_6 soluble reaction products following ^{13}CO addition to **5-Na**. The insets show enlargements of the resonances attributable to carbonyl complexes P2Mo(^{13}CO)$_3$ [**C**] and P2Mo(^{13}CO) [**D**]. Significant decomposition to free diphopshine [**P2**] is observed.

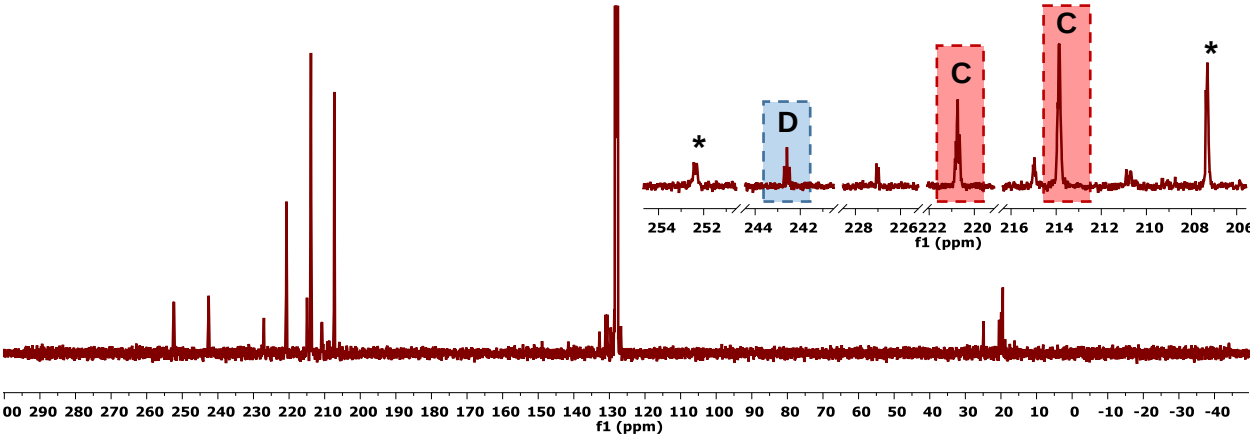

Figure S5—$^{13}C\{^{1}H\}$ NMR spectrum (126 MHz, C_6D_6, 25 °C) of the C_6H_6 soluble reaction products following ^{13}CO addition to **5-Na**. The inset shows an enlargement of the resonances attributable to carbonyl complexes P2Mo($^{13}CO)_3$ [**C**] and P2Mo(^{13}CO) [**D**]. Unidentified ^{13}C containing byproducts are designated with an asterisk (*).

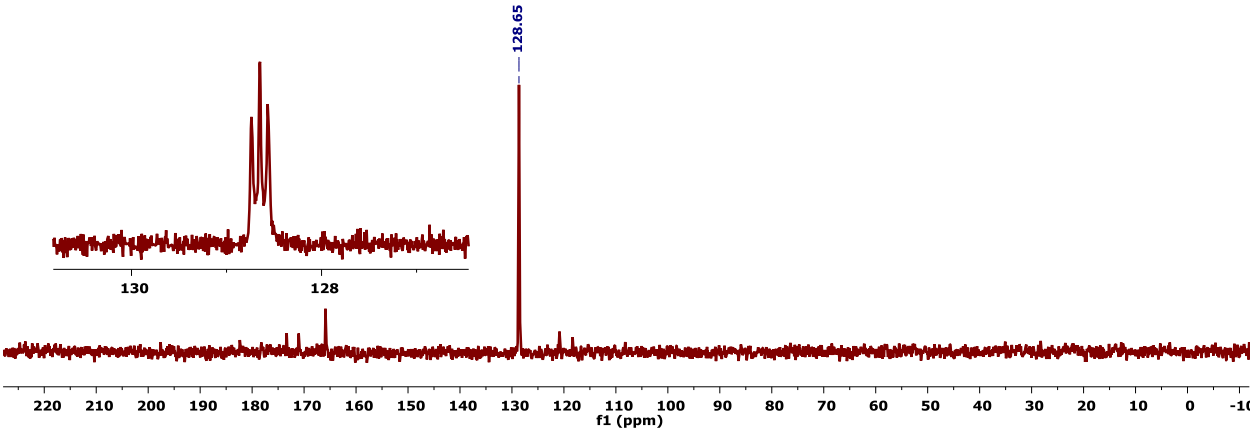

Figure S6—$^{13}C\{^{1}H\}$ NMR spectrum (126 MHz, C_6D_6, 25 °C) of the D_2O soluble reaction products following ^{13}CO addition to **5-Na**. The inset shows the triplet attributable to $NaN^{13}CO$ (^{1}J(N,C) = 11.34 Hz).

Plausible Mechanisms for Nitride/CO Coupling

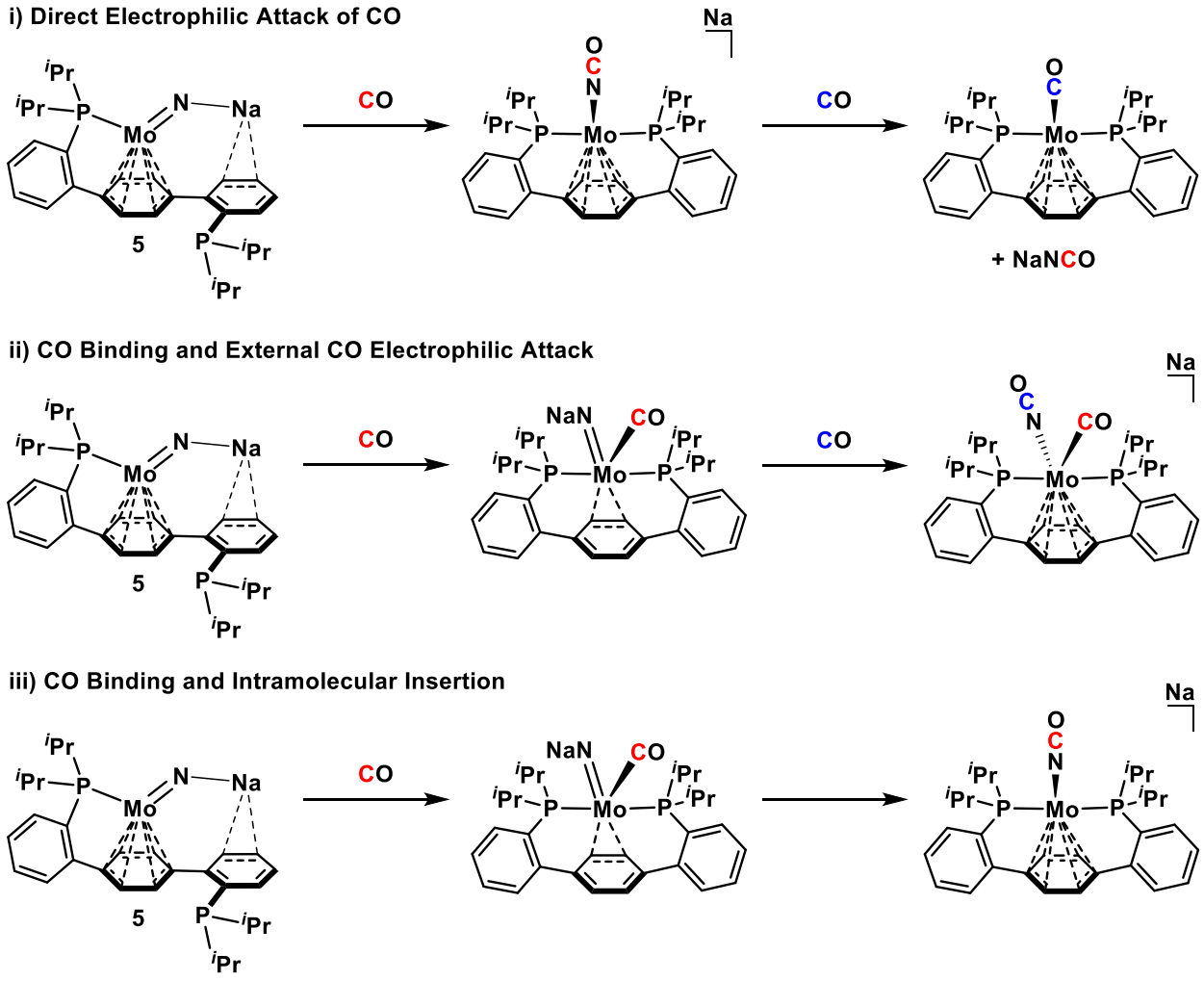

Scheme S1—Possible mechanisms for cyanate anion formation from **5-Na** and CO.

NMR Spectra

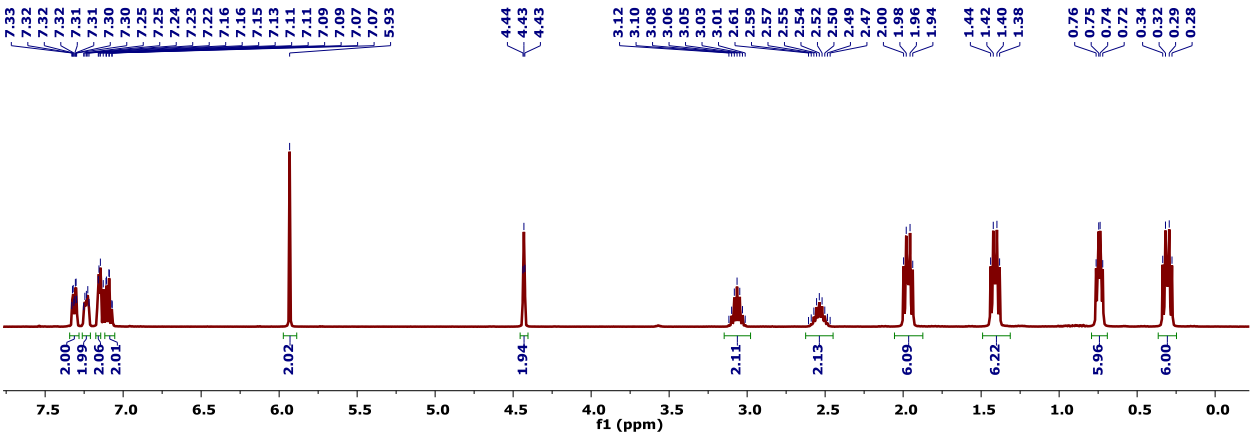

Figure S7—^{1}H NMR spectrum (400 MHz, C_6D_6, 23 °C) of **2**.

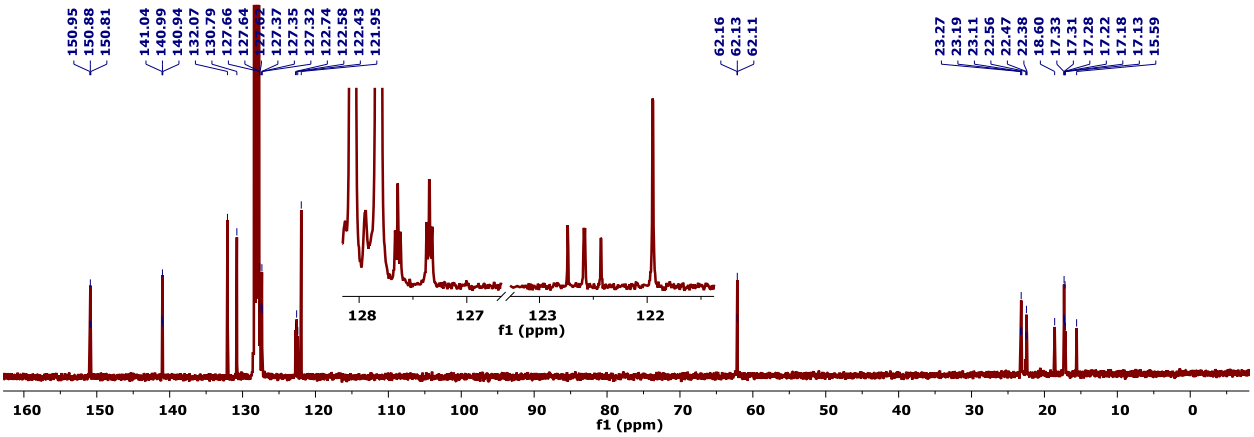

Figure S8—^{13}C{^{1}H} NMR spectrum (101 MHz, C_6D_6, 23 °C) of **2**. The inset depicts and enlargement of the aromatic region.

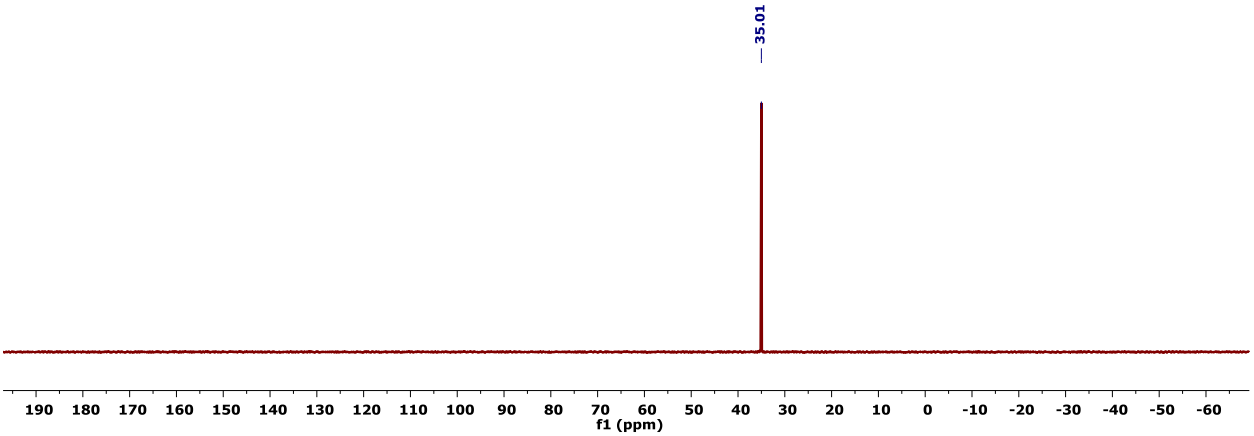

Figure S9—^{31}P{^{1}H} NMR spectrum (162 MHz, C_6D_6, 23 °C) of **2**.

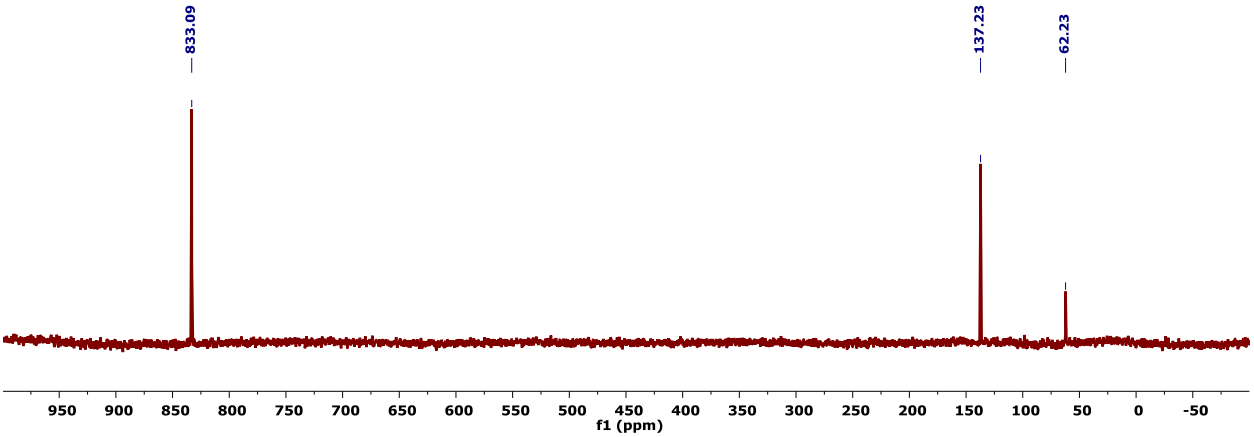

Figure S10—$^{15}N\{^{1}H\}$ NMR spectrum (51 MHz, C_6D_6, 25 °C) of **2**.

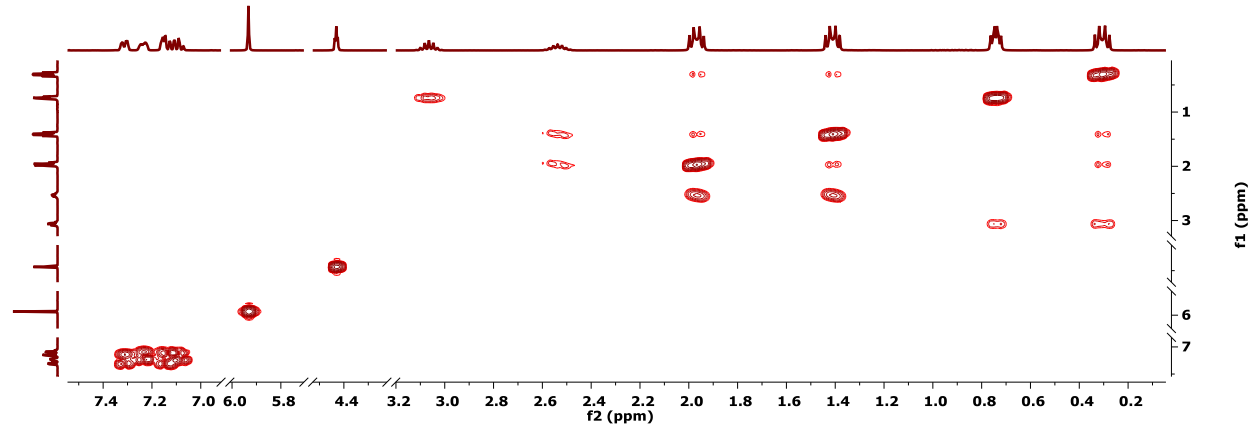

Figure S11—$^{1}H/^{1}H$ COSY NMR spectrum (400 MHz, C_6D_6, 23 °C) of **2**.

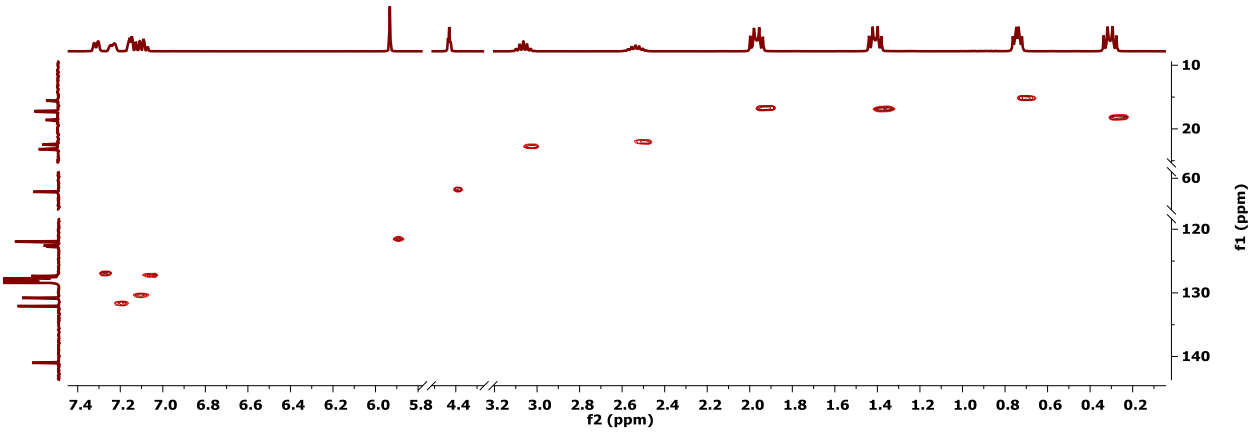

Figure S12—$^{1}H/^{13}C$ HSQC NMR spectrum (400/101 MHz, C_6D_6, 23 °C) of **2**.

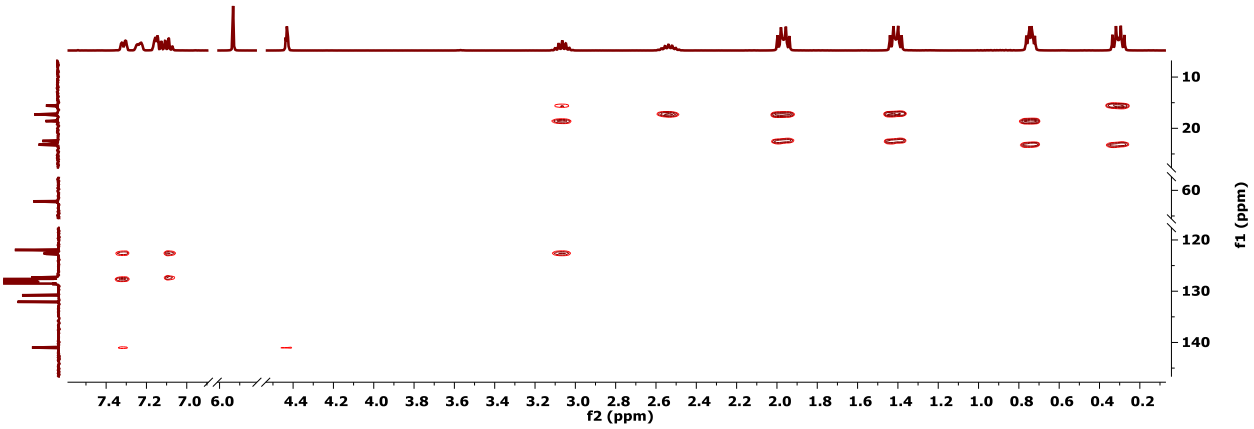

Figure S13—$^{1}H/^{13}C$ HMBC NMR spectrum (400/101 MHz, C_6D_6, 23 °C) of **2**.

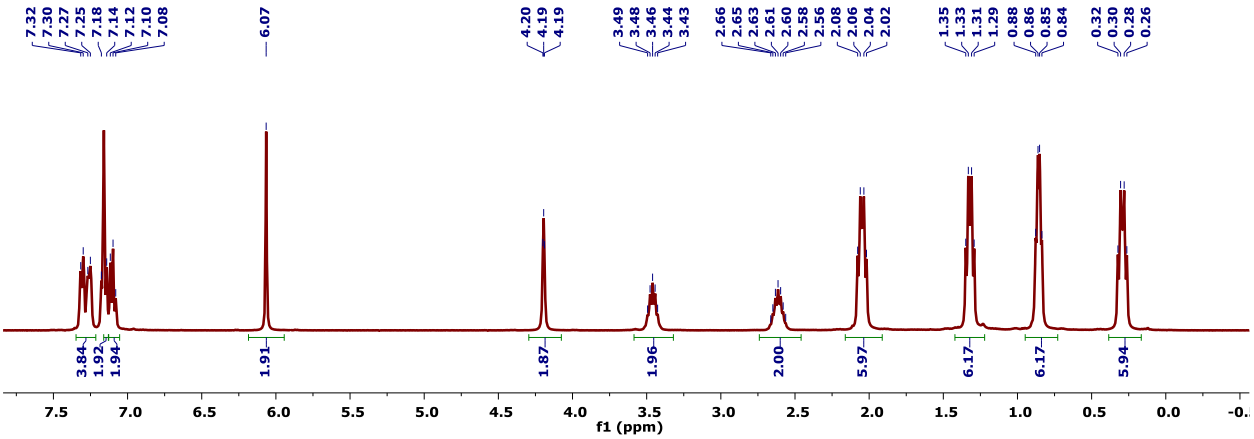

Figure S14—^{1}H NMR spectrum (400 MHz, C_6D_6, 23 °C) of **3**.

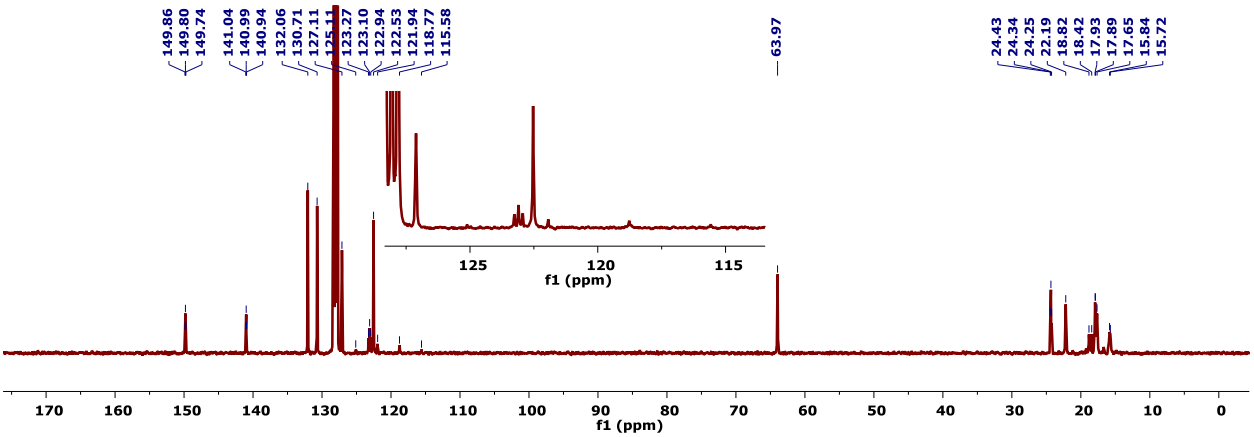

Figure S15—$^{13}C\{^{1}H\}$ NMR spectrum (101 MHz, C_6D_6, 23 °C) of **3**. The inset depicts and enlargement of the aromatic region.

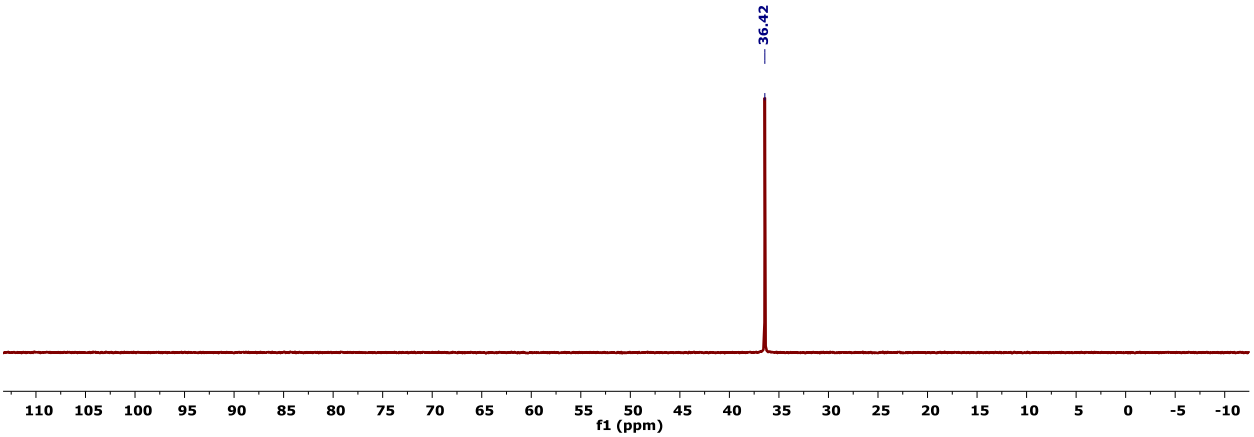

Figure S16—$^{31}P\{^{1}H\}$ NMR spectrum (162 MHz, C_6D_6, 23 °C) of **3**.

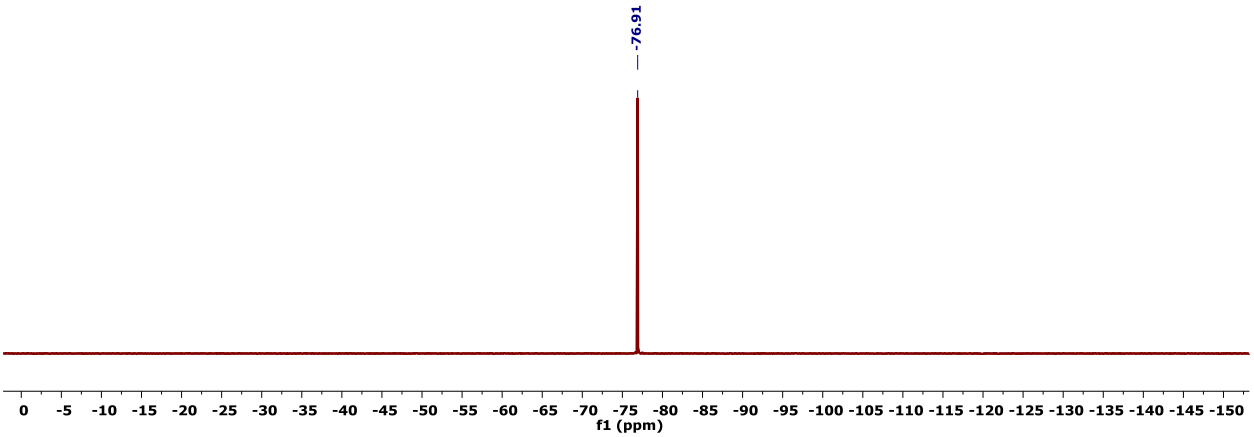

Figure S17—^{19}F NMR spectrum (376 MHz, C_6D_6, 23 °C) of **3**.

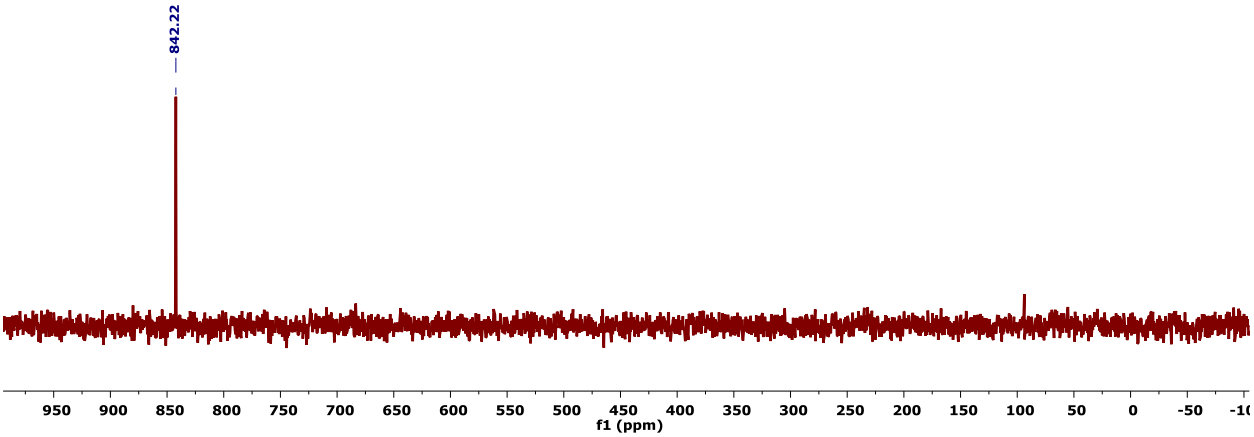

Figure S18—$^{15}N\{^{1}H\}$ NMR spectrum (51 MHz, C_6D_6, 25 °C) of **3**.

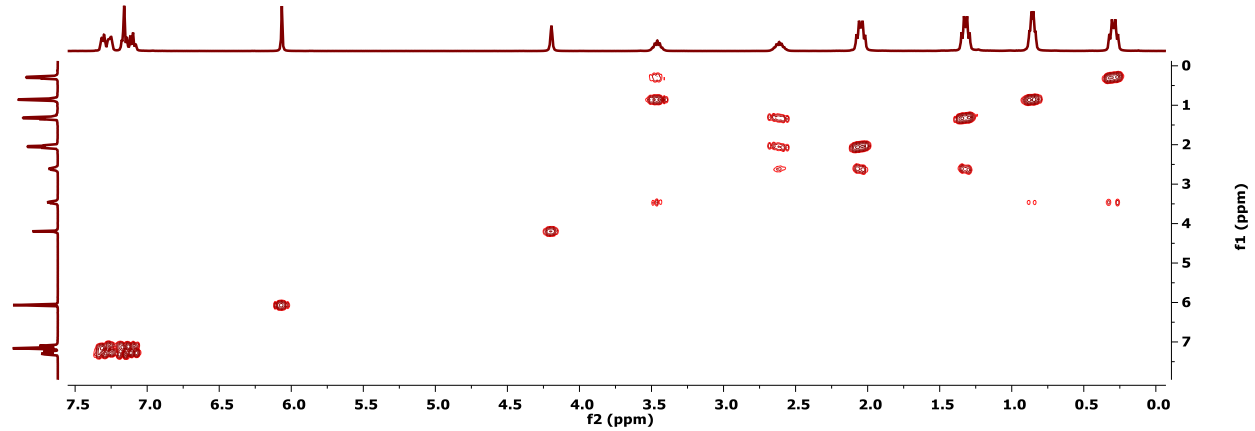

Figure S19—$^{1}H/^{1}H$ COSY NMR spectrum (400 MHz, C_6D_6, 23 °C) of **3**.

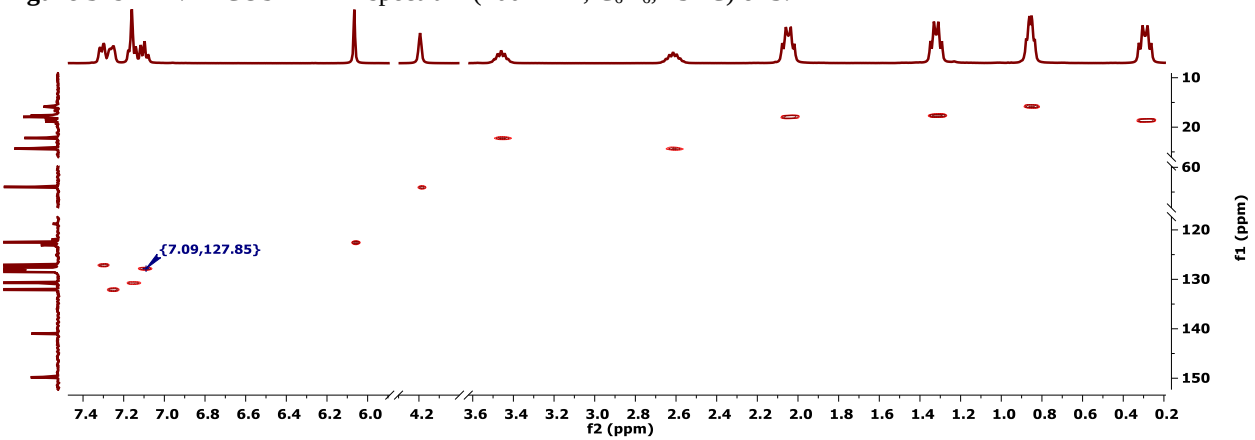

Figure S20—$^{1}H/^{13}C$ HSQC NMR spectrum (400/101 MHz, C_6D_6, 23 °C) of **3**. The ^{13}C resonance that coincides with the C_6D_6 solvent residual is labeled.

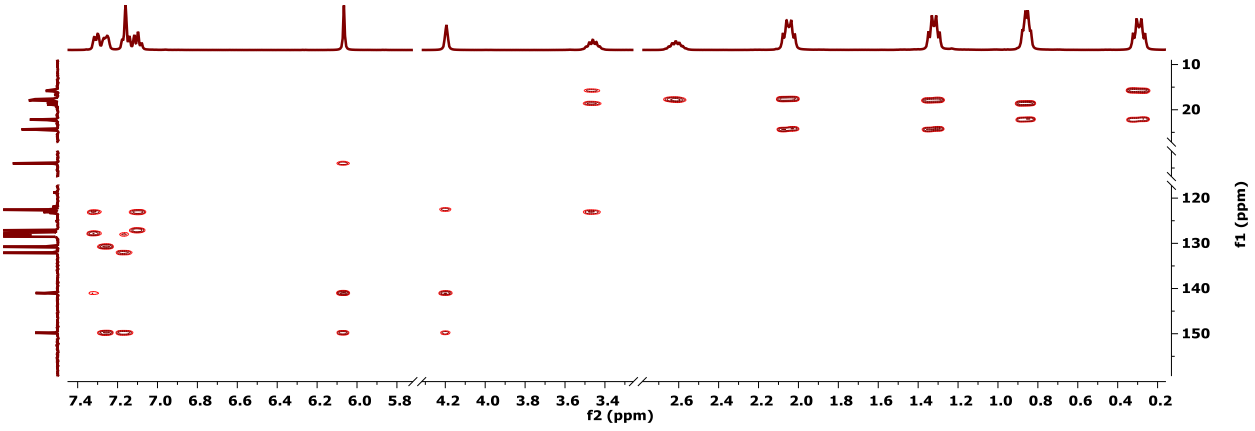

Figure S21—$^{1}H/^{13}C$ HMBC NMR spectrum (400/101 MHz, C_6D_6, 23 °C) of **3**.

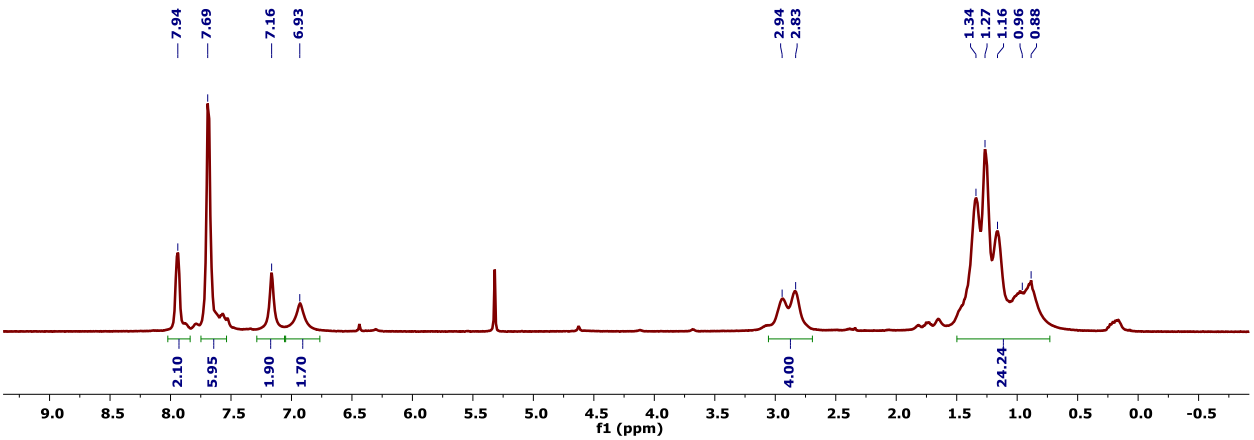

Figure S22—^{1}H NMR spectrum (400 MHz, CD_2Cl_2, 23 °C) of a reaction mixture comprised primarily of **4-^{13}C**.

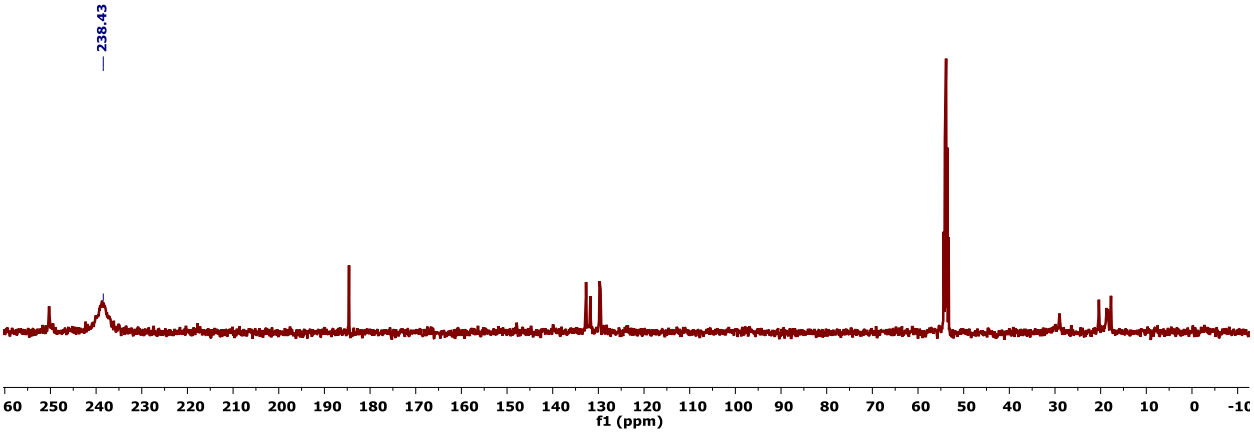

Figure S23—^{13}C{^{1}H} NMR spectrum (101 MHz, CD_2Cl_2, 23 °C) of a reaction mixture comprised primarily of **4-^{13}C**. The sufficient spectral signal to noise was obtained to validate the broad resonance for the isotopically enriched carbonyl.

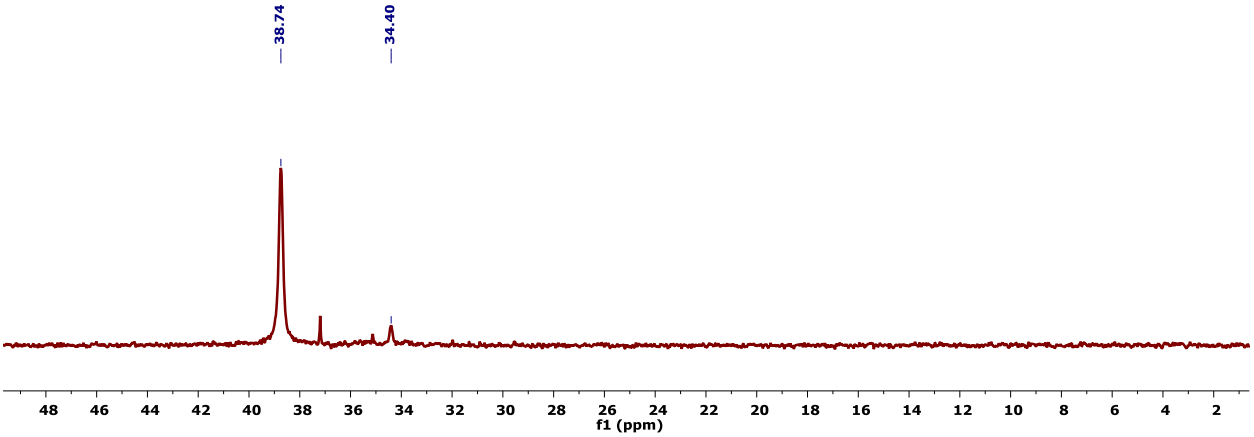

Figure S24—^{31}P{^{1}H} NMR spectrum (162 MHz, CD_2Cl_2, 23 °C) of a reaction mixture comprised primarily of **4-^{13}C**.

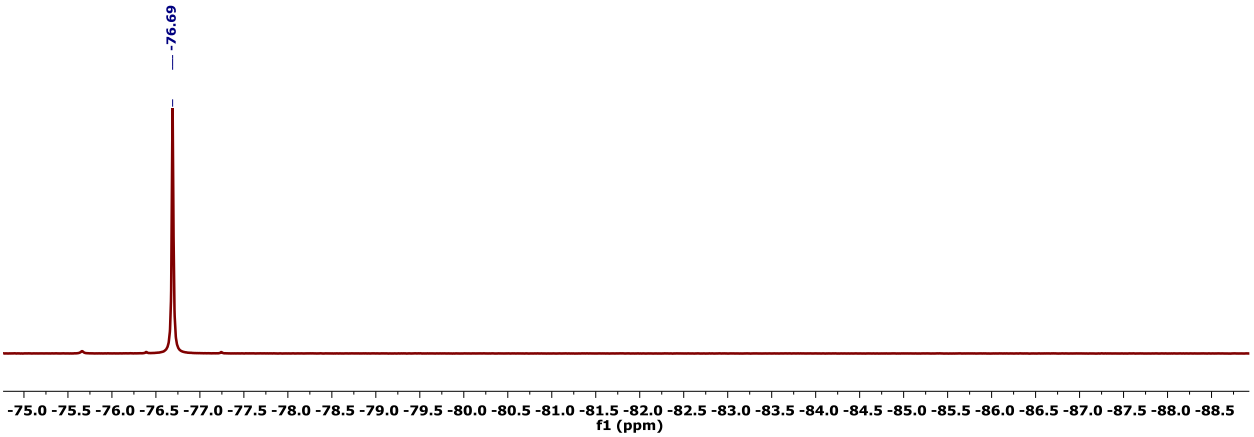

Figure S25—^{19}F NMR spectrum (376 MHz, CD_2Cl_2, 23 °C) of a reaction mixture comprised primarily of **4-^{13}C**.

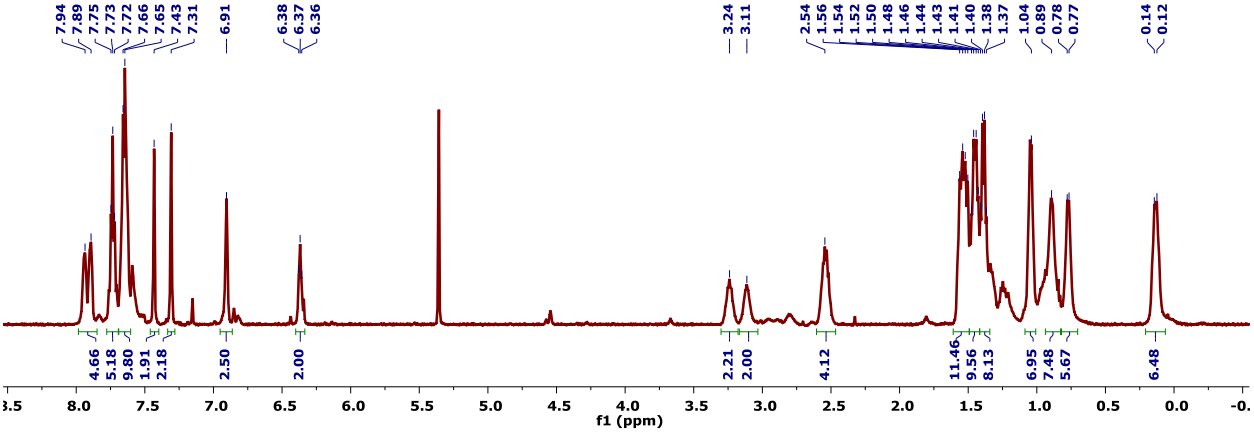

Figure S26—^{1}H NMR spectrum (500 MHz, CD_2Cl_2, -65 °C) of a reaction mixture comprised primarily of **4-^{13}C**.

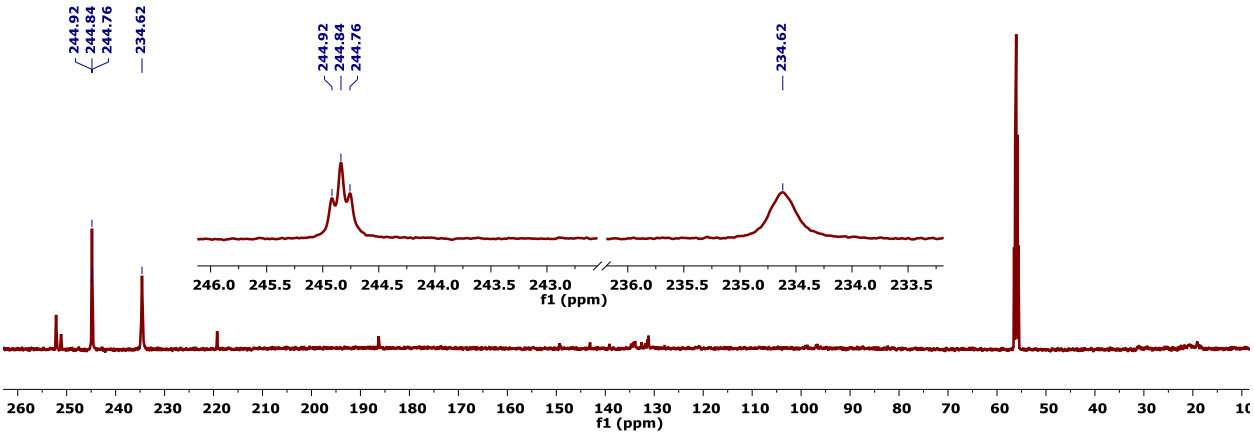

Figure S27—^{13}C{^{1}H} NMR spectrum (126 MHz, CD_2Cl_2, -65 °C) of a reaction mixture comprised primarily of **4-^{13}C**. The sufficient spectral signal to noise was obtained to validate the broad resonance for the isotopically enriched carbonyl. The inset shows enlargements of the CO resonances of the two isomers of **4-^{13}C**.

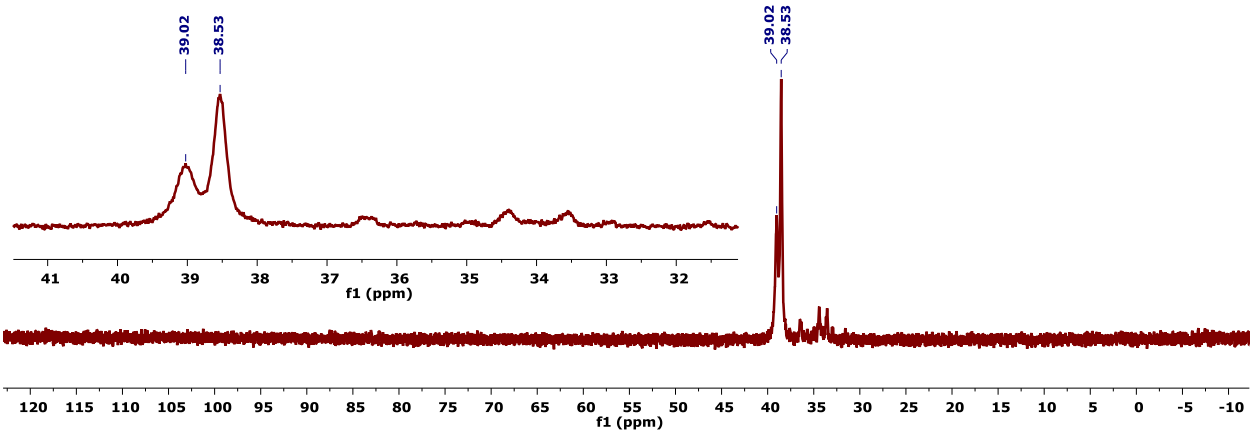

Figure S28—$^{31}P\{^{1}H\}$ NMR spectrum (202 MHz, CD_2Cl_2, -65 °C) of a reaction mixture comprised primarily of **4-^{13}C**. The inset highlights the two resonances attributable to **4-^{13}C**.

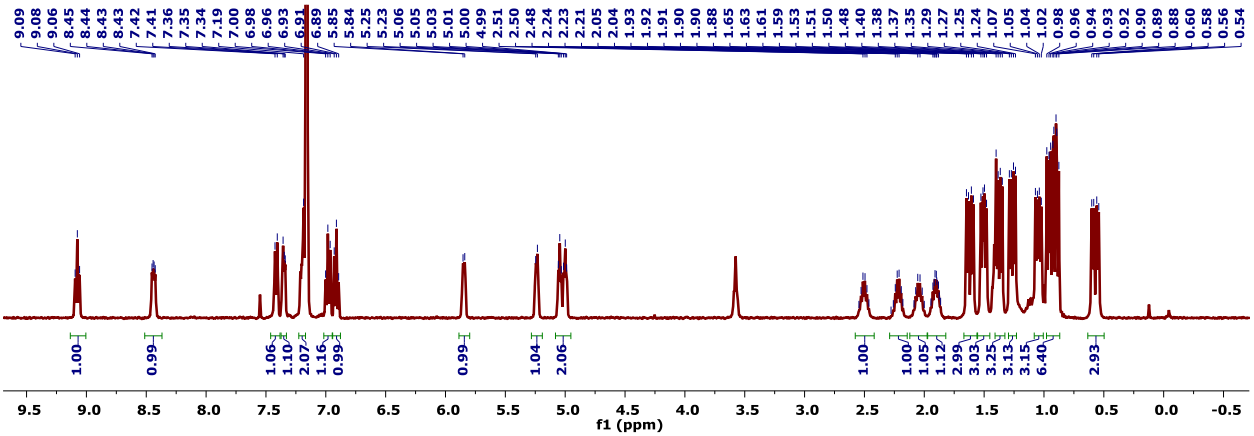

Figure S29—^{1}H NMR spectrum (400 MHz, C_6D_6, 23 °C) of **5**.

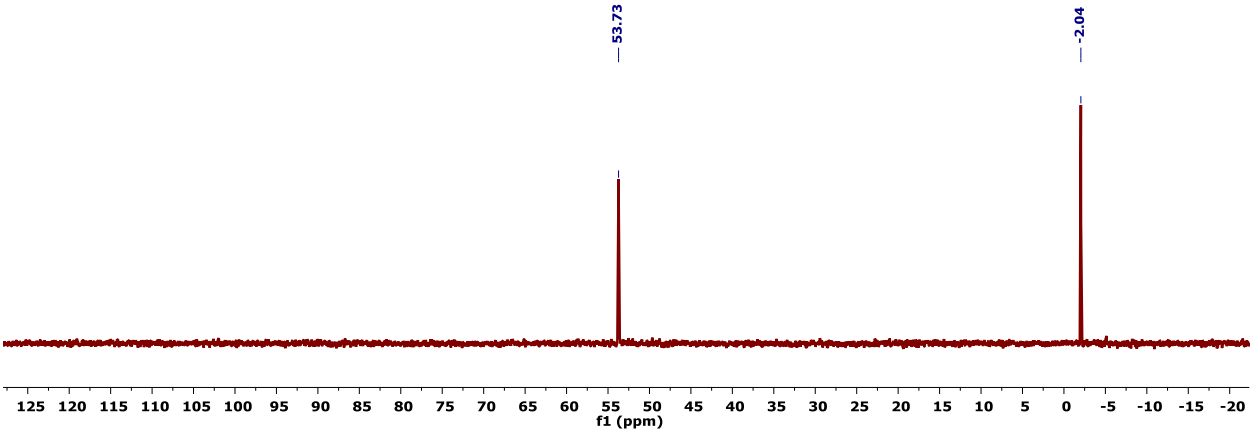

Figure S30—$^{31}P\{^{1}H\}$ NMR spectrum (162 MHz, C_6D_6, 23 °C) of **5**.

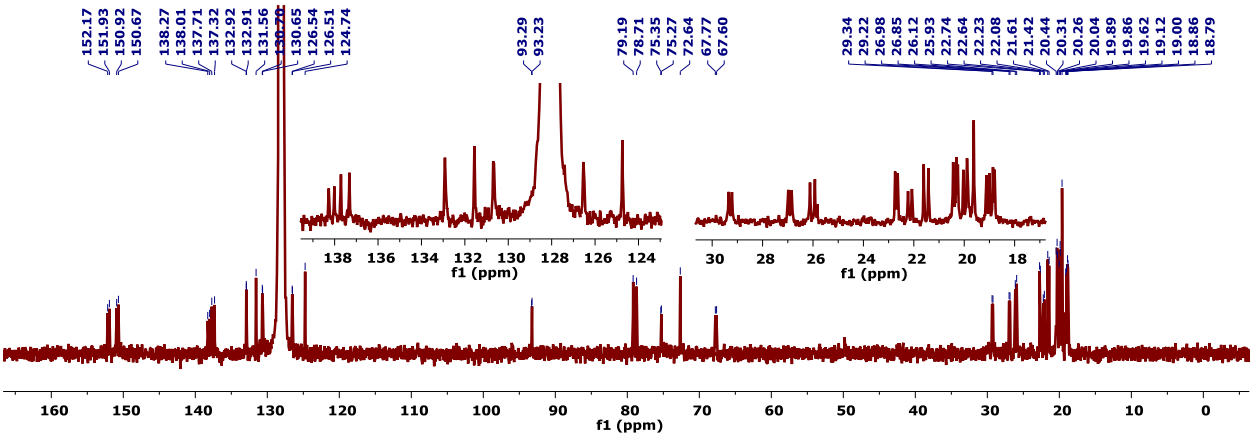

Figure S31—$^{13}C\{^{1}H\}$ NMR spectrum (101 MHz, C_6D_6, 23 °C) of **5**. The insets show the enlargements of the aromatic (left) and aliphatic (right) regions of the spectrum.

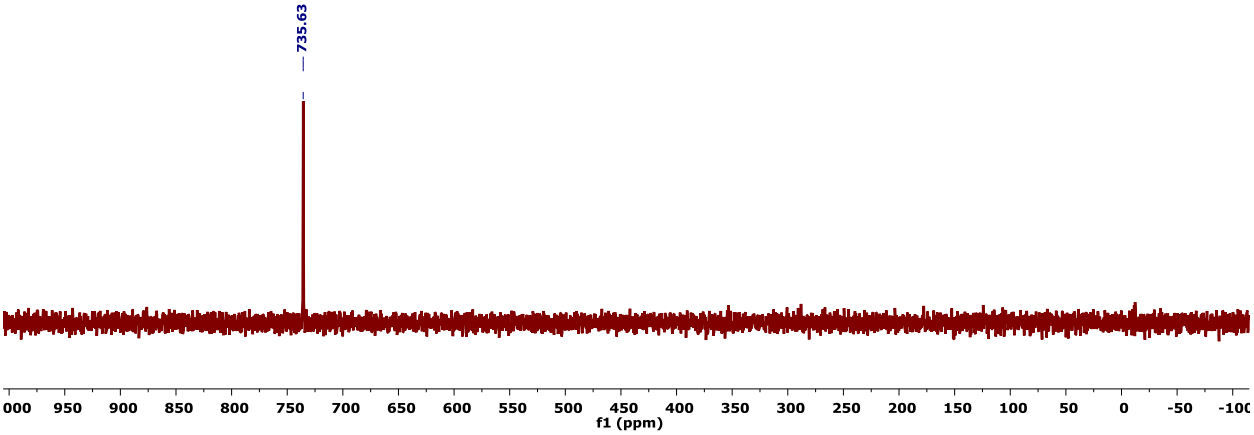

Figure S32—$^{15}N\{^{1}H\}$ NMR spectrum (51 MHz, C_6D_6, 25 °C) of **5**.

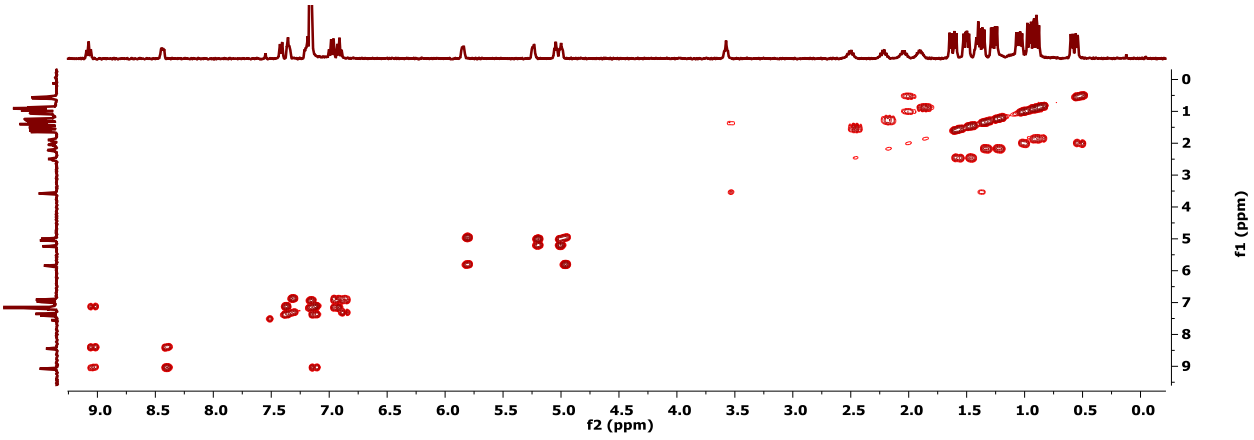

Figure S33—$^{1}H/^{1}H$ COSY NMR spectrum (400 MHz, C_6D_6, 23 °C) of **5**.

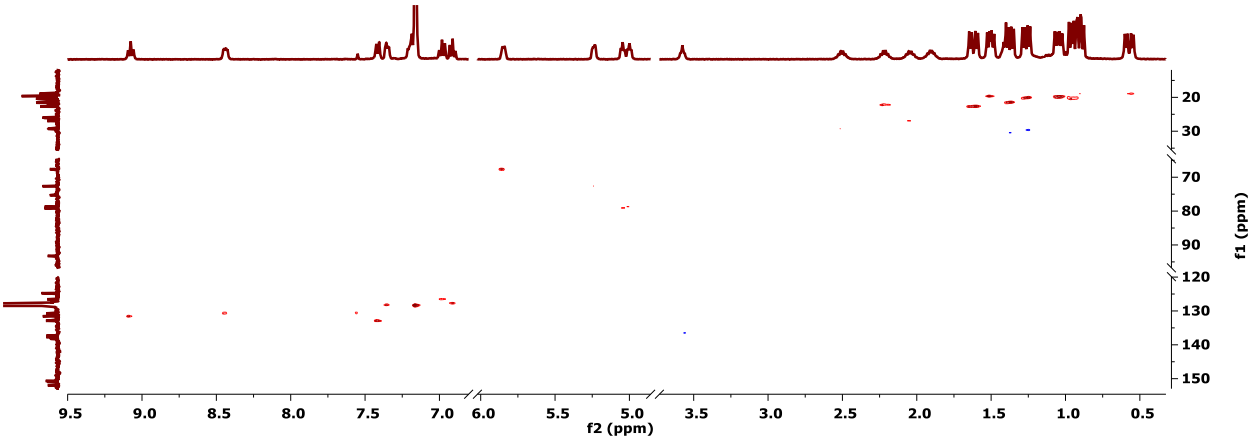

Figure S34—$^{1}H/^{13}C$ HSQC NMR spectrum (400/101 MHz, C_6D_6, 23 °C) of **5**.

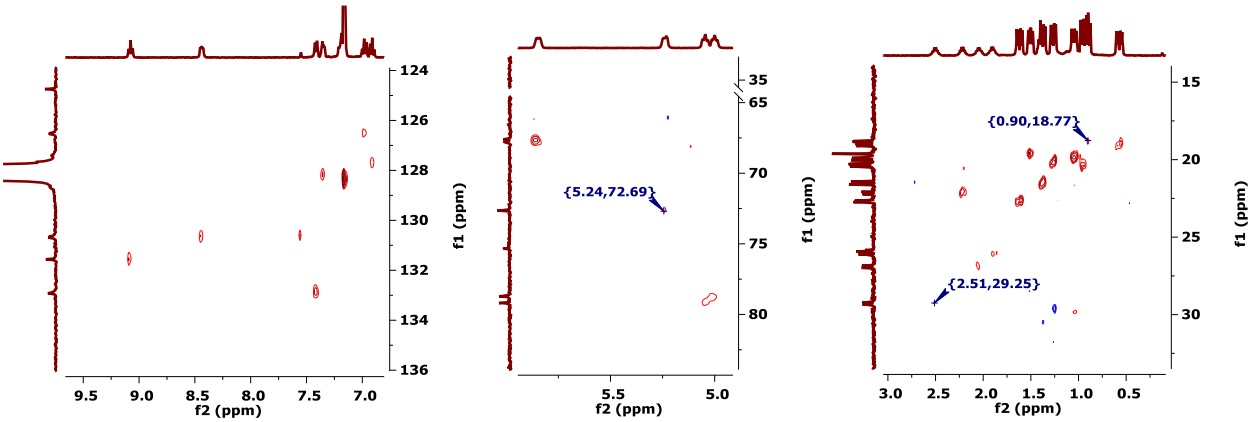

Figure S35—Partial $^{1}H/^{13}C$ HSQC NMR spectra (400/101 MHz, C_6D_6, 23 °C) of **5**.

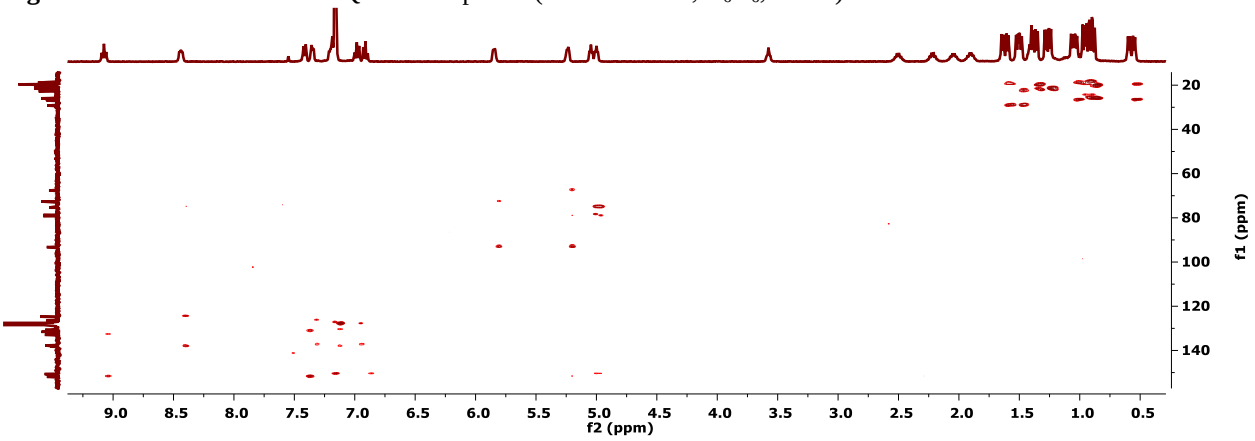

Figure S36—$^{1}H/^{13}C$ HMBC NMR spectrum (400/101 MHz, C_6D_6, 23 °C) of **5**.

Computational Details

All calculations were performed with DFT as implemented in Gaussian 09 Revision C.01.[4] Geometry optimizations and electronic structure calculations were performed with revised TPSS exchange and correlation functionals.[5] The LANL2DZ basis set was used for all atoms.[6] No solvent corrections were employed. All optimizations were performed ignoring molecular symmetry—crystallographic coordinates were used as a starting point—for complex **3**, the solid state structure of **2** was modified, replacing the N_3 ligand with a coordinated OTf. Energetic minima were confirmed with subsequent frequency calculations which did not return imaginary frequencies. Structures optimized in this manner showed good agreement with bond lengths and angles determined via single crystal X-ray diffraction (Table S1). Molecular orbital and spin density illustrations were generated using GaussView, the GUI component of the Gaussian software package, and depicted with 0.05 e/Å^3 or 0.001 e/Å^3 isosurface values, respectively.

Table S1—Comparison of Experimental and Calculated Structural Metrics for **5**.

	5		
	Exp.	**Calc.**	Δ
Mo1–N1	1.728(2)	1.745	-0.02
Mo1–P1	2.518(1)	2.570	-0.05
Mo1–C1	2.432(3)	2.568	-0.14
Mo1–C2	2.284(3)	2.403	-0.12
Mo1–C3	2.230(3)	2.237	-0.01
Mo1–C4	2.266(3)	2.276	-0.01
Mo1–C5	2.245(3)	2.250	-0.01
Mo1–C6	2.370(3)	2.441	-0.07
C1–C2	1.422(5)	1.440	-0.02
C2–C3	1.433(4)	1.455	-0.02
C3–C4	1.419(5)	1.479	-0.06
C4–C5	1.446(5)	1.484	-0.04
C5–C6	1.427(5)	1.451	-0.02
C6–C1	1.394(5)	1.437	-0.04
N1–K1	2.733(3)	2.646	0.09

Cartesian Coordinates for 5

Mo	0.831000	-0.753000	-0.249000
P	3.321000	-0.541000	0.353000
P	-3.844000	1.136000	0.821000
N	0.738000	-2.443000	0.176000
C	1.487000	1.704000	-0.609000
C	1.159000	1.059000	-1.851000
H	1.841000	1.126000	-2.694000
C	-0.075000	0.313000	-2.011000
H	-0.344000	-0.022000	-3.007000
C	-1.082000	0.282000	-0.921000
C	-0.644000	0.801000	0.393000
H	-1.322000	0.795000	1.238000
C	0.618000	1.513000	0.523000
H	0.883000	1.934000	1.488000
C	2.895000	2.176000	-0.396000
C	3.889000	1.241000	0.034000
C	5.237000	1.659000	0.162000
H	6.007000	0.945000	0.451000
C	5.605000	2.997000	-0.104000
H	6.646000	3.305000	-0.001000
C	4.622000	3.928000	-0.508000
H	4.900000	4.962000	-0.714000
C	3.280000	3.514000	-0.658000
H	2.520000	4.222000	-0.987000
C	-2.318000	-0.514000	-1.107000
C	-3.559000	-0.356000	-0.360000
C	-4.612000	-1.288000	-0.576000
H	-5.545000	-1.169000	-0.026000
C	-4.531000	-2.348000	-1.509000
H	-5.374000	-3.024000	-1.651000
C	-3.357000	-2.457000	-2.299000
H	-3.272000	-3.236000	-3.058000
C	-2.293000	-1.564000	-2.099000
H	-1.378000	-1.707000	-2.669000
C	3.771000	-0.946000	2.207000
H	3.451000	-1.998000	2.287000
C	5.266000	-0.835000	2.595000
H	5.920000	-1.405000	1.919000
H	5.411000	-1.234000	3.612000
H	5.595000	0.213000	2.601000
C	2.881000	-0.097000	3.148000
H	3.139000	0.971000	3.077000
H	3.028000	-0.416000	4.193000
H	1.821000	-0.216000	2.885000
C	4.601000	-1.606000	-0.645000
H	5.613000	-1.302000	-0.329000
C	4.375000	-3.108000	-0.332000
H	4.635000	-3.356000	0.708000
H	5.003000	-3.724000	-0.995000
H	3.320000	-3.375000	-0.495000
C	4.429000	-1.313000	-2.156000
H	3.409000	-1.569000	-2.478000
H	5.144000	-1.918000	-2.737000
H	4.606000	-0.252000	-2.384000
C	-5.478000	0.649000	1.761000
H	-6.257000	0.319000	1.056000
C	-6.004000	1.902000	2.515000
H	-5.222000	2.329000	3.162000
H	-6.859000	1.625000	3.151000
H	-6.341000	2.685000	1.821000
C	-5.176000	-0.494000	2.768000
H	-4.834000	-1.407000	2.257000
H	-6.081000	-0.748000	3.343000
H	-4.395000	-0.183000	3.479000
C	-4.521000	2.466000	-0.452000
H	-4.845000	3.290000	0.206000
C	-5.719000	2.002000	-1.314000
H	-5.433000	1.157000	-1.957000
H	-6.049000	2.827000	-1.966000
H	-6.581000	1.695000	-0.702000
C	-3.355000	2.979000	-1.337000
H	-2.509000	3.331000	-0.731000
H	-3.706000	3.814000	-1.965000
H	-2.986000	2.185000	-1.999000
K	-1.795000	-3.012000	0.687000

Crystallographic Information

CCDC deposition numbers 1833019-1833021 contain the supplementary crystallographic data for this paper. These data can be obtained free of charge from The Cambridge Crystallographic Data Centre via www.ccdc.cam.ac.uk/data_request/cif.

Refinement Details

In each case, crystals were mounted on a MiTeGen loop using Paratone oil, then placed on the diffractometer under a nitrogen stream. Low temperature (100 K) X-ray data were obtained on a Bruker KAPPA APEXII CCD based diffractometer (Mo fine-focus sealed X-ray tube, K_α = 0.71073 Å) or a Bruker D8 VENTURE Kappa Duo PHOTON 100 CMOS based diffractometer (Mo $I_\mu S$ HB micro-focus sealed X-ray tube, K_α = 0.71073 Å). All diffractometer manipulations, including data collection, integration, and scaling were carried out using the Bruker APEXIII software.[7] Absorption corrections were applied using SADABS.[8] Space groups were determined on the basis of systematic absences and intensity statistics and the structures were solved in the Olex 2 software interface[9] by intrinsic phasing using XT (incorporated into SHELXTL)[10] and refined by full-matrix least squares on F^2. All non-hydrogen atoms were refined using anisotropic displacement parameters. Hydrogen atoms were placed in the idealized positions and refined using a riding model, unless noted otherwise. The structures were refined (weighed least squares refinement on F^2) to convergence. Graphical representations of structures with 50% probability thermal ellipsoids were generated using the Diamond 3 visualization software.[11]

Table S4—Crystal and refinement data for complexes **2, 4**, & **5**.

	2	**4**	**5**
CCDC Number[12]	1833019	1833020	1833021
Empirical formula	$C_{37}H_{48}MoN_4P_2$	$C_{32}H_{40}F_3MoNO_4P_2S$	$C_{138}H_{178}K_4Mo_4N_4P_8$
Formula weight	706.67	749.59	2680.75
T (K)	100	100	100
a, Å	8.5855(3)	13.2525(4)	17.7072(8)
b, Å	27.9202(11)	12.0007(3)	35.4203(15)
c, Å	14.8976(6)	21.5895(6)	21.8165(10)
α, °	90	90	90
β, °	99.246(2)	104.4510(10)	101.582(3)
γ, °	90	90	90
Volume, Å^3	3524.7(2)	3324.94(16)	13404.6(10)
Z	4	4	4
Crystal system	Monoclinic	Monoclinic	Monoclinic
Space group	$P2_1/n$	$P2_1/c$	$P2_1/n$
d_{calc}, g/cm^3	1.332	1.497	1.328
θ range, °	2.012 to 45.374	2.324 to 40.418	1.307 to 31.589
μ, mm^{-1}	0.494	0.607	0.634
Abs. Correction	Semi-empirical	Semi-empirical	Semi-empirical
GOF	1.061	1.034	1.010
R_1,[a] wR_2 [b] [I>2 σ(I)]	0.0294, 0.0722	0.0331, 0.0674	0.0579, 0.0934
Radiation Type	Mo K_α	Mo K_α	Mo K_α

[a] $R_1 = \sum||F_o| - |F_c||/\sum|F_o|$. [b] $wR_2 = [\sum[w(F_o^2-F_c^2)^2]/\sum[w(F_o^2)^2]^{1/2}$.

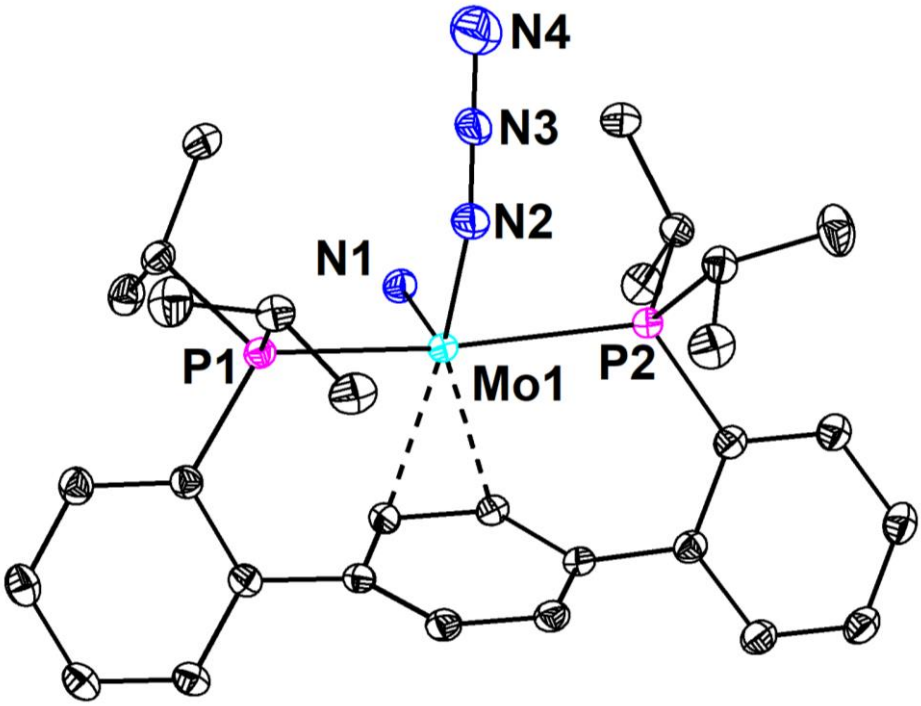

Figure S30—Structural drawing of **2** with 50% probability anisotropic displacement ellipsoids. H-atoms are omitted for clarity.

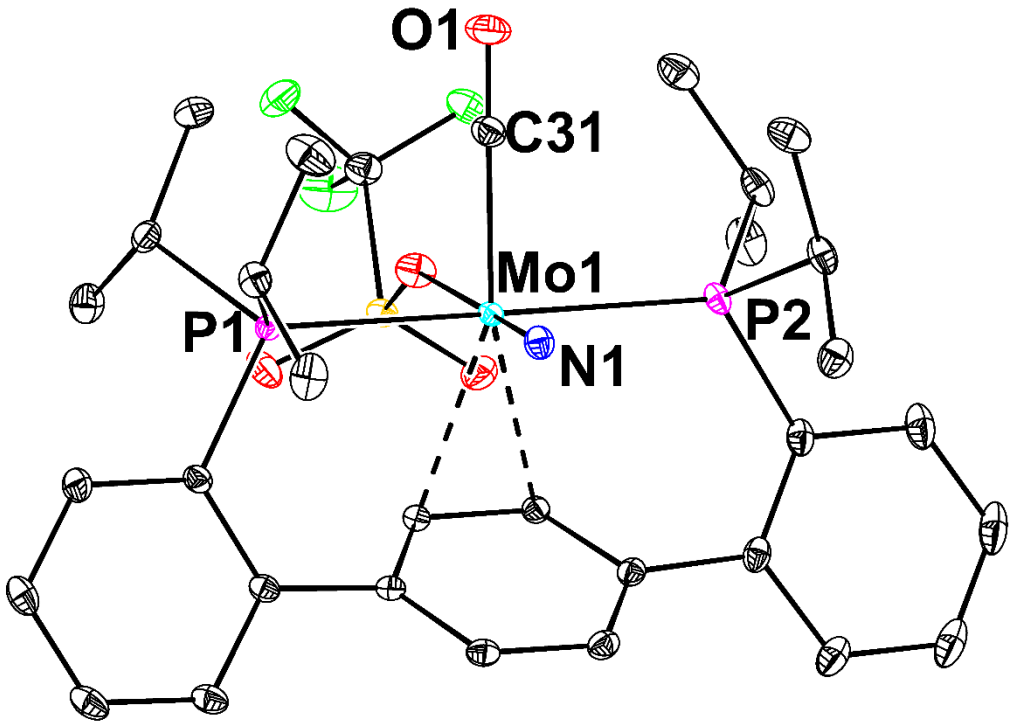

Figure S31—Structural drawing of **4** with 50% probability anisotropic displacement ellipsoids. H-atoms are omitted for clarity.

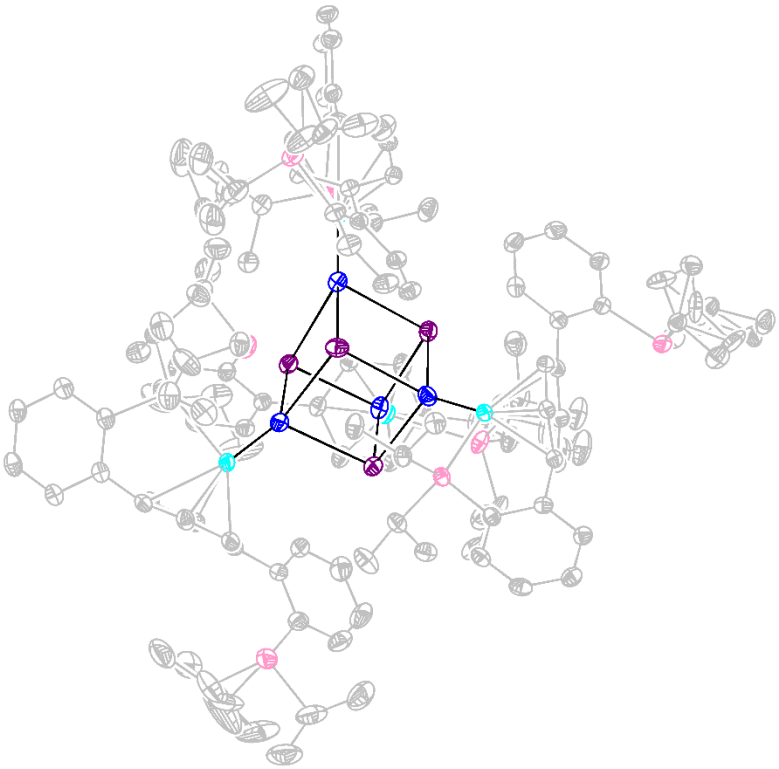

Figure S32—Structural drawing of **5** with 50% probability anisotropic displacement ellipsoids. H-atoms and benzene solvate molecules are omitted for clarity. Atoms of the *para*-terphenyl diphosphine ancillary ligand have been deemphasized for clarity.

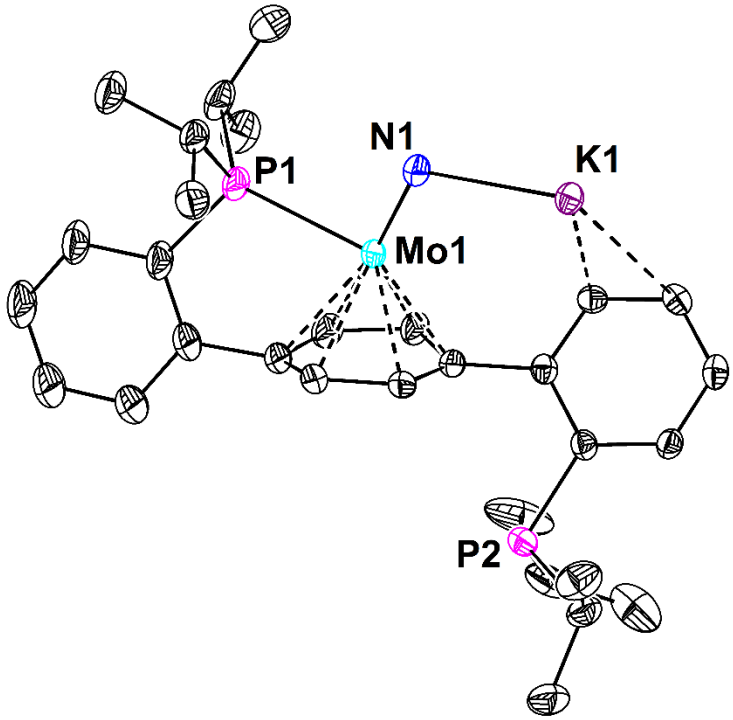

Figure S32—Structural drawing of a single P2MoNK unit of **5** with 50% probability anisotropic displacement ellipsoids. H-atoms and benzene solvate molecules are omitted for clarity.

Special Refinement Details:

Six of the phosphine isopropyl groups were positionally disordered. These disorders were satisfactorily modeled in two discreet positions with relative populations as follows: C55A/B through C57A/B (80/20), C58A/B through C60A/B (80/20), C80A/B and C81A/B (62/38), C88A/B through C90A/B (75/25), C115/215 through C117/217 (42/58), and C118/218 through C120/220 (56/44). Additionally, the two diisopropyl phosphine motifs (P6 and C85 through C90B, P8 and C115 through C220) were refined with similarity restraints on U_{ij} and rigid bond restraints.

References

(1) Pangborn, A. B.; Giardello, M. A.; Grubbs, R. H.; Rosen, R. K.; Timmers, F. J. *Organometallics* **1996**, *15*, 1518.
(2) Buss, J. A.; Edouard, G. A.; Cheng, C.; Shi, J.; Agapie, T. *J. Am. Chem. Soc.* **2014**, *136*, 11272.
(3) Fulmer, G. R.; Miller, A. J. M.; Sherden, N. H.; Gottlieb, H. E.; Nudelman, A.; Stoltz, B. M.; Bercaw, J. E.; Goldberg, K. I. *Organometallics* **2010**, *29*, 2176.
(4) Gaussian 09, Revision C.01, Frisch, M. J.; Trucks, G. W.; Schlegel, H. B.; Scuseria, G. E.; Robb, M. A.; Cheeseman, J. R.; Scalmani, G.; Barone, V.; Mennucci, B.; Petersson, G. A.; Nakatsuji, H.; Caricato, M.; Li, X.; Hratchian, H. P.; Izmaylov, A. F.; Bloino, J.; Zheng, G.; Sonnenberg, J. L.; Hada, M.; Ehara, M.; Toyota, K.; Fukuda, R.; Hasegawa, J.; Ishida, M.; Nakajima, T.; Honda, Y.; Kitao, O.; Nakai, H.; Vreven, T.; Montgomery, Jr., J. A.; Peralta, J. E.; Ogliaro, F.; Bearpark, M.; Heyd, J. J.; Brothers, E.; Kudin, K. N.; Staroverov, V. N.; Kobayashi, R.; Normand, J.; Raghavachari, K.; Rendell, A.; Burant, J. C.; Iyengar, S. S.; Tomasi, J.; Cossi, M.; Rega, N.; Millam, J. M.; Klene, M.; Knox, J. E.; Cross, J. B.; Bakken, V.; Adamo, C.; Jaramillo, J.; Gomperts, R.; Stratmann, R. E.; Yazyev, O.; Austin, A. J.; Cammi, R.; Pomelli, C.; Ochterski, J. W.; Martin, R. L.; Morokuma, K.; Zakrzewski, V. G.; Voth, G. A.; Salvador, P.; Dannenberg, J. J.; Dapprich, S.; Daniels, A. D.; Farkas, Ö.; Foresman, J. B.; Ortiz, J. V.; Cioslowski, J.; Fox, D. J. Gaussian, Inc., Wallingford CT, 2009.
(5) a) Perdew, J. P.; Ruzsinszky, A.; Csonka, G. I.; Constantin, L. A.; Sun, J. *Phys. Rev. Lett.* **2011**, *106*, 179902; b) Perdew, J. P.; Ruzsinszky, A.; Csonka, G. I.; Constantin, L. A.; Sun, J. *Phys. Rev. Lett.* **2009**, *103*, 026403.
(6) a) Wadt, W. R.; Hay, P. J. *J. Chem. Phys.* **1985**, *82*, 284; b) Hay, P. J.; Wadt, W. R. *J. Chem. Phys.* **1985**, *82*, 299; c) Hay, P. J.; Wadt, W. R. *J. Chem. Phys.* **1985**, *82*, 270; d) Dunning, T. H.; Hay, P. J. In *Methods of Electronic Structure Theory*; Schaefer, H. F., Ed.; Springer US: Boston, MA, 1977, p 1.
(7) APEX3, Version 1 User Manual, M86-EXX229, Bruker Analytical X-ray Systems, Madison, WI, May 2016.
(8) Sheldrick, G.M. "SADABS (version 2008/1): Program for Absorption Correction for Data from Area Detector Frames", University of Göttingen, 2008.
(9) Dolomanov, O. V.; Bourhis, L. J.; Gildea, R. J.; Howard, J. A. K.; Puschmann, H. *J. Appl. Cryst.* **2009**, *42*, 339.
(10) Sheldrick, G.M. *Acta Cryst.* **2008**, *A64*, 112.
(11) Brandenburg, K. (1999). DIAMOND. Crystal Impact GbR, Bonn, Germany.
(12) Crystallographic data have been deposited at the CCDC, 12 Union Road, Cambridge CB2 1EZ, UK and copies can be otained on request, free of charge, by quoting the publication citation and the respective deposition numbers.